UNIVERSITÀ DEGLI STUDI DI PADOVA

UNIVERSITÀ DEGLI STUDI DI PADOVA
Dipartimento di Ingegneria Industriale DII
Corso di Laurea Magistrale in Ingegneria Aerospaziale

AEROACOUSTIC ANALYSIS OF A UHBR ENGINE WITH A VARIABLE AREA NOZZLE USING SEMI-EMPIRICAL METHODS

Relatore: Prof. Andrea Magrini

Laureando: Alessio Piccinini, 2053750

Anno Accademico 2023/2024

ABSTRACT

The civil aviation industry is currently moving towards engines with higher bypass ratios to improve environmental sustainability and operational efficiency. Variable area nozzles are a critical component of these technologies, providing dynamic adjustments to optimise engine performance under different operating conditions. The objective of this study is to perform an analysis of the aeroacoustic performance of a high bypass ratio turbofan engine equipped with a variable geometry nozzle. The approach adopted is based on the use of semi-empirical models, in particular those implemented in CHalmers nOIse Code (CHOICE), an open source aircraft noise estimation framework. Specifically, the Sound Pressure Level (SPL) at the source and at the microphone are evaluated for the jet, the fan and the whole aircraft. Considerations on the Effective perceived noise level (EPNL) for noise regulations are presented. The analysis focuses on the three designated noise certification points for a commercial aircraft: approach, sideline and cutback. In each of these scenarios, the effect of the variable geometry nozzle on noise emissions is studied, allowing a quantitative assessment of its impact in the context of each operational phase. A reduction in jet noise of up to -1.4 dB can be achieved with a nozzle opening of 20%. Similarly, fan noise can be reduced by up to -2 dB. The greatest reduction in total aircraft noise is achieved with a -1 dB difference.

SOMMARIO

L'industria dell'aviazione civile è in continua evoluzione verso l'adozione di motori turbofan con elevato rapporto di bypass, mirando a migliorare le prestazioni ambientali ed operative. In questo contesto, gli ugelli a geometria variabile rivestono un ruolo fondamentale, permettendo ottimizzazioni nelle prestazioni del motore in diverse condizioni operative. Lo scopo di questo studio è condurre un'analisi aeroacustica su un motore con elevato rapporto di bypass dotato di ugello a geometria variabile. L'approccio adottato si basa sull'utilizzo di modelli semi-empirici, specificatamente quelli integrati in CHOICE, un framework open source per la stima del rumore di un velivolo. In particolare, il livello di pressione sonora è valutato alla sorgente e al microfono per il getto, fan e l'intero aeromobile. Inoltre, viene valutato anche l'EPNL (Equivalent Perceived Noise Level) al fine di valutare la conformità alle normative sul livello di rumore. L'analisi si concentra infatti sulle tre fasi di certificazione sonora per un velivolo commerciale: approach, sideline e cutback. In ciascuna di queste fasi si analizza l'effetto della geometria variabile sul rumore emesso dalle diverse sorgenti, giungendo ad una valutazione quantitativa per ogni fase operativa. Con'apertura del 20% dell'area di bypass, si osserva una riduzione del rumore del getto pari a -1.4 dB. In maniera simile il rumore generato dal fan registra una diminuzione di -2 dB. La riduzione più importante per l'aereo completo si trova essere invece di -1 dB.

CONTENTS

LIST OF FIGURES

LIST OF TABLES

ABBREVIATIONS

ANOPP Aircraft Noise Prediction Program.

BPR Bypass Ratio.

CDA Continuous Descent Approach.

CFD Computational Fluid Dynamics.

CHOICE CHalmers nOIse Code.

DAC Dual annular combustor.

EPNL Effective perceived noise level.

FPR Fan Pressure Ratio.

ICAO International Civil Aviation Organisation.

IGV Inlet guide vanes.

ISA International Standard Atmosphere.

MLW Maximum Landing Weight.

MTOW Maximum Take-off Weight.

NADP Noise Abatement Departure Procedure.

NASA CRM-HL NASA High Lift Common Research Model.

OASPL Overall Sound Pressure Level.

PANAM Parametric Aircraft Noise Analysis Module, DLR.

PNL Perceived Noise Level.

rms Root mean square.

ROC Rate of Climb.

RSS Rotor stator spacing.

SPL Sound Pressure Level.

TAS True Air Speed.

UHBR Ultra high bypass ratio.

VAN Variable Area Nozzle.

NOMENCLATURE

A_{18} Nozzle bypass area.

A_8 Nozzle core area.

C_D Drag Coefficient.

C_L Lift Coefficient.

$M_{\mathbf{trd}}$ Rotor tip relative inlet Mach number at the design point.

$M_{\mathbf{tr}}$ Rotor tip relative inlet Mach number at the operating point.

T_{18} Nozzle bypass total temperature.

T_8 Nozzle core total temperature.

V_{18} Nozzle bypass velocity.

V_8 Nozzle core velocity.

α angle of attack.

γ flight path angle.

θ angle of rotation.

1 PROBLEM OVERVIEW

The aviation industry's need for more fuel-efficient aircraft, driven by economic and environmental concerns, has led to the introduction of engines with larger bypass ratios. When introducing new technology, it is important to carefully assess all the implications. In addition to engine emissions, noise is another issue to consider. Regulations are becoming increasingly restrictive [20], as noise has been shown to cause health problems for people living near airports[21]. The following chapters present an aeroacoustic analysis of a UHBR engine with a Variable Area Nozzle (VAN). It is known from theory [14] that noise reduction is expected as the bypass area increases, so the aim of this study is to obtain a quantitative result of the effect of this implementation on engine noise. For this purpose, 9 different nozzle bypass areas are considered, ranging from 90% of the nominal area to 120%. For each configuration, the noise results are analysed in terms of source SPL, perceived SPL and EPNL. The analysis starts with the engine noise source alone and then moves to the whole aircraft, which is the NASA CRM-HL, for the three acoustic certification points. This chapter presents the essential acoustic parameters for understanding sound propagation in air and a description of all the problems associated with the study. It also provides a brief presentation of the different methods available for noise estimation, as presented by [22], and lays the groundwork for the following chapters. Chapter 2 describes the case study and the framework used, including the engine and aircraft details required for noise estimation and defines the trajectories used for the certification points. Chapter 3 presents the results for the different configurations considered, in particular the certification points. Finally, Chapter 4 presents conclusions and future developments.

1.1 Acoustic parameters

Before going into the details of aircraft noise and related regulations, the main parameters used throughout the study are described. The aim is to predict the acoustic perturbation responsible for the noise at the listener's position, i.e. the pressure variation p' that deviates from the mean ambient pressure p0 and is perceived by the ear (i.e. by the ear (i.e. $p = p0 + p'$). Thus, acoustics deals with small perturbations of a flow that allow the linearisation of the governing equations [23]. We focus on the pressure perturbations p' that can be perceived by the human ear:

$$p'(t) := p(t) - p_0 \tag{1.1}$$

in Pascal. The steady part p_0 of the pressure $p(t)$ is the temporal average, not perceived auditively:

$$p_0 = p := \lim_{T\to\infty} \frac{1}{T} \int_{-\frac{T}{2}}^{\frac{T}{2}} p(t)\, dt \tag{1.2}$$

An appropriate measure for the strength of an acoustical signal is the Root mean square (rms) value $\tilde{p}$ of the sound pressure:

$$\tilde{p} = \sqrt{\overline{p'^2}} \tag{1.3}$$

For harmonic pressure fluctuations the audio range is:

$$20\,\mathrm{Hz} \leq f \leq 20\,\mathrm{kHz} \tag{1.4}$$

Aircraft noise prediction is often restricted to a narrower band and in our case:

$$50\,\mathrm{Hz} \leq f \leq 10\,\mathrm{kHz} \tag{1.5}$$

The SPL, measured in decibel (dB), quantifies the pressure deviation caused by a sound source and is given by:

$$SPL = 20\log_{10}\left(\frac{p'_{\mathrm{rms}}}{p_{\mathrm{ref}}}\right) \tag{1.6}$$

where $p_{\mathrm{ref}} = 2 \cdot 10^{-5}$ Pa for sound propagating in air, which corresponds to the threshold of hearing for humans.

1.1.1 Noise weighting

To gain a better understanding of certification limits, it is important to consider that the sensitivity of the human ear depends strongly on the frequency of the perceived sound. Therefore, two pure tones with the same sound pressure level but different frequencies will be perceived as having different loudness.

The loudness level LN of a pure tone of a given frequency $f = \omega/(2\pi)$ and a given sound pressure level $Lp(f)$ is defined as the sound pressure level of the pure 1000 Hz tone that is perceived as equally loud. The loudness is defined as:

$$s := 2(LN40)/10, [s] = sone \tag{1.7}$$

and is a measure for the intensity perception. This last equation demonstrates how the loudness level can be computed based on a given loudness value:

$$LN = 40 + 33.2lg(s) \tag{1.8}$$

Figure 1.1a shows that certain frequencies are perceived as noisier than others, depending on the physiology of the human ear, even with the same LN. Therefore, to obtain a simple measure of the perceived sound, a process of noise weighting is necessary. Lp is weighted in a frequency-dependent manner, using one of the internationally agreed weightings (e.g. A-, B-, C-, D-), as shown in Figure 1.1b.

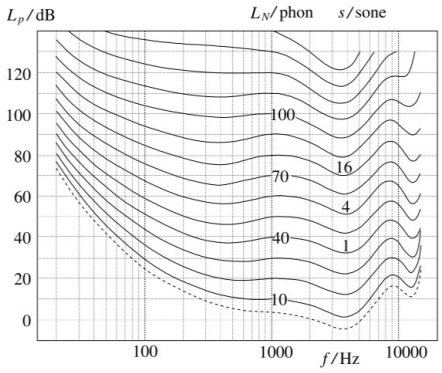

(a) Loudness Level contours [24].

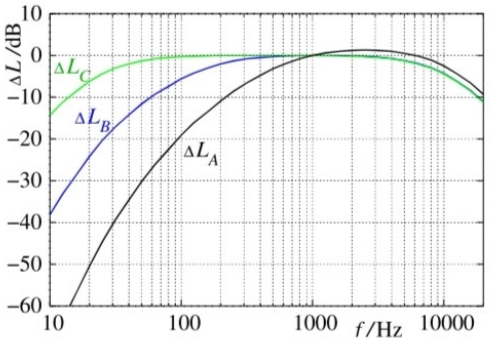

(b) Noise weighting curves [24].

In particular, these are useful for the EPNL computation.

1.1.2 EPNL calculation

For regulatory terms, the Sound Pressure Level (SPL) in the one-third octave band i is measured at intervals of 0.5 s for every time step k. The measured sound pressure level (SPL) is frequency-weighted using the Noy tables [24]. The individual one-third octave bands are then summed over i to obtain the Total Perceived Noisiness N(k), which is then converted to the Perceived Noise Level (PNL) for each time step. To account for the human hearing sensitivity to discrete tones, a sound correction known as C(k) is applied, resulting in the Tone-Corrected Perceived Noise Level, i.e. PNLT(k). The Equivalent Perceived Noise Level (EPNL) is then calculated by integrating all levels of PNLT(k) over time.

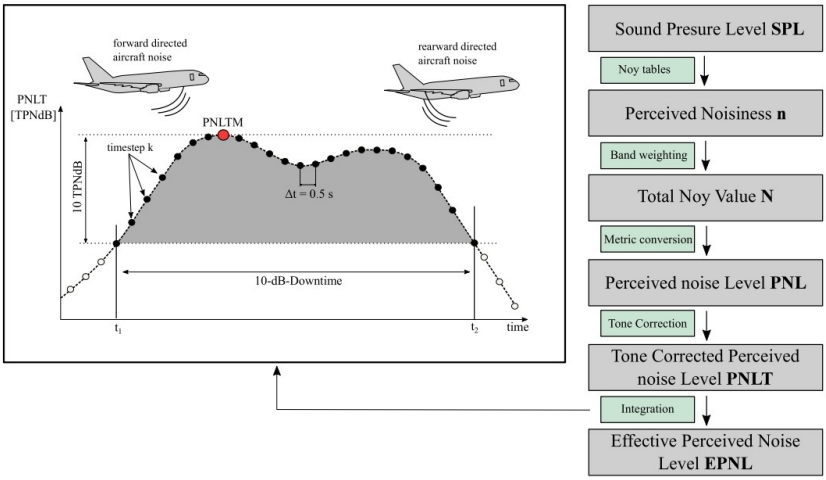

Figure 1.2: EPNL calculation [1]

1.2 Aircraft noise and regulations

Although individual aircraft have become much less noisy over the last 30 years, the growth in air traffic means that many citizens are still exposed to high levels of noise. This exposure makes noise one of a number of environmental challenges for the development of future aircraft and the improvement of those already in use. In fact, aircraft noise has been linked not only to annoyance but also to more serious health problems [21]. Regulations have been developed by the International Civil Aviation Organisation (ICAO) with the Annex 16 [20], with continuous and increasingly stringent updates as shown in Figure 1.3.

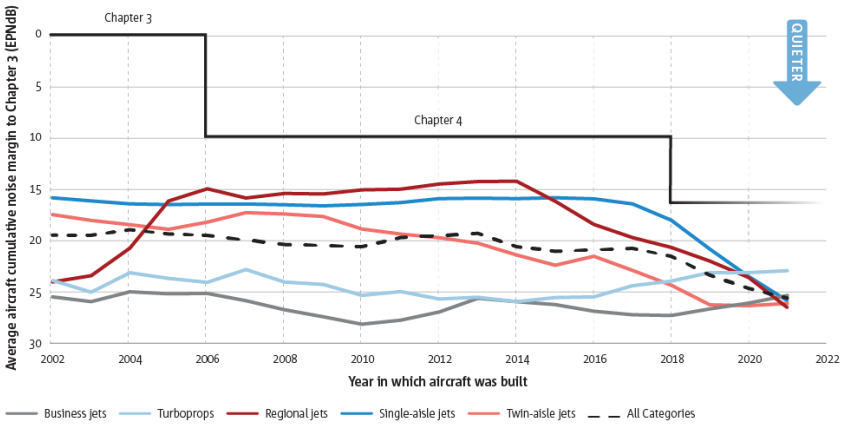

Figure 1.3: Regulations time frame [2]

In particular, the phases of flight that are subject to strict regulations are those at lower altitudes, i.e. approach, sideline and cutback.

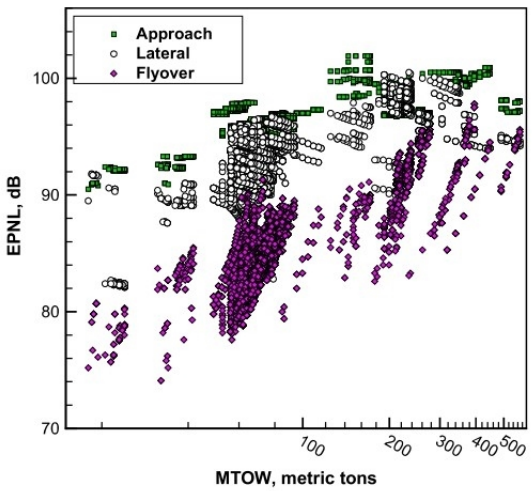

Figure 1.4: Recorded EPNL on approach, lateral (sideline), flyover (takeoff) [2]

The different phases are regulated by a maximum EPNL depending on the Maximum Take-off Weight (MTOW). Figure 1.4 shows the recorded EPNL for the three cases for different MTOW, while figure 1.5 shows the reference points for the noise certification.

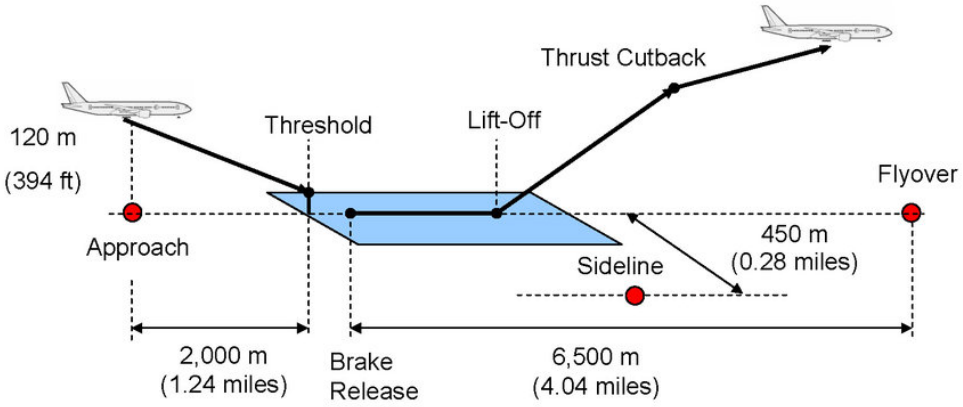

Figure 1.5: Certification points [3]

For example we take the Boeing 777-300ER due to its similarity to the aircraft considered in this study and from [2] we get the maximum EPNL reported in table 1.1.

Certification point	EPNL Limit (dB)
Approach	105
Sideline	102.5
Cutback	100.5

Table 1.1: B777-300ER EPNL limitations

We proceed describing in a more accurate way the three phases.

1.2.1 Approach

During approach, the dominant airframe source contributions are from the landing gear, high-lift devices, control surfaces and drag augmentation devices, while the dominant engine noise typically originates from the fan and low pressure turbine [**?**]. The sound pressure level from all noise sources is also logarithmically proportional to $1/(distance)^2$. Steeper approach angles therefore reduce the noise impact by keeping aircraft at a higher altitude for a given distance from touchdown. One of the most promising operational techniques for approach noise abatement in the current Air Traffic Control (ATC) system involves Continuous Descent Approach (CDA) procedures that eliminate level segments, keeping aircraft higher and at lower thrust levels for longer than conventional "step-down" approach techniques. This significantly reduces noise impacts by a noticeable amount in the approach phase. Most current approaches are performed at 3 degrees, although some airports require steeper angles due to stricter

regulations. ICAO defines the approach noise measurement standard as shown in figure 1.6. Specifically, the aircraft must follow a CDA with a glide ratio $\gamma = -3\,\mathrm{deg}$ and must be at 120 m above the microphone positioned at 2000 m from the landing threshold.

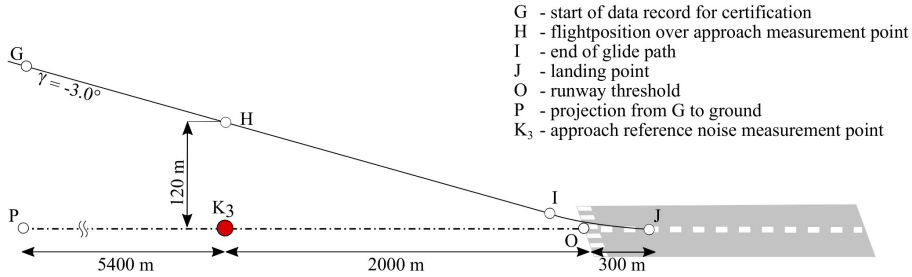

Figure 1.6: Approach reference measurement [1]

1.2.2 Sideline and Cutback

Unlike the standard approach procedure, the take-off procedure allows more freedom. In fact, aircraft must follow the safety instructions of the manufacturer and reach predetermined speeds. From a noise regulatory point of view, two measurement points are established. One is the cutback reference noise measurement point (K1 in figure 1.10), with the microphone positioned 6500 m after the brake release point, while the other is a full power sideline reference, with an array of microphones positioned on a line 450 m parallel to the runway centreline out of which the one who registers the loudest sound is considered. After reaching the respective cutback altitude, the aircraft must climb at least with 4%, which corresponds to a climb angle of approximately $2.29\,\mathrm{deg}$ and the flight must be recorded up to 11 km after the brake release point.

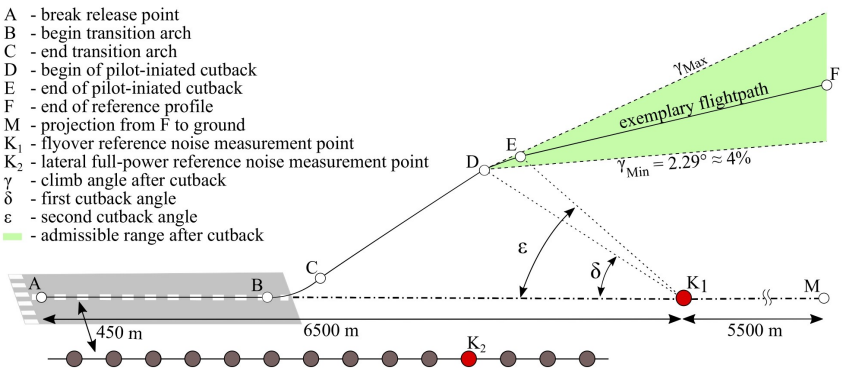

Figure 1.7: Take-off reference measurements [1]

1.3 Noise mitigation

From an operational aspect it is not realistic to think of redesigning entire fleets that were thought to operate beyond 2050. Although studies and initiatives have been developed such as the Silent Aircraft Initiative [25] which has the objective of drastically reducing the aircraft noise to 62 dB in the vicinity of airports, there is the need to develop adjustments to the existing aircraft. There are a number of ways to reduce the noise generated :

- noise reduction at the source
- Improvements in flight procedures
- Restriction of operations

In particular, the VAN influences both fan and jet noise which are, for this reason, the main focus of the study.

1.3.1 Noise reduction at the source

Engine noise is one of the major contributors to the overall sound levels as aircraft operate near airports. Turbofan engines are commonly used on commercial transports due to their advantage for higher performance and lower noise. The noise reduction comes from combinations of changes to the engine cycle parameters and low-noise design features. Engine noise sources principally come from the fan (including the stator), the exhaust (also referred to as the jet), the compressor, the combustor, and the turbine. For modern large aircraft, Single Aisle and Twin Aisle, jet noise is a secondary noise source even at departure, with fan noise dominating [26]. In particular we focus on VAN technology. The trend towards higher bypass ratios in commercial gas turbine engines has widened the operating gap between fan flow conditions at different flight speeds. This necessitates the use of variable geometry to maintain the surge margin throughout the flight envelope. Mechanisms such as a variable area nozzle are employed to help maintain the surge margin, particularly as engine bypass ratio increases. To maintain the optimum design ratio between the bypass ratio (BPR) and the ratio of jet velocities from the core and bypass streams, a decrease in the fan pressure ratio (FPR) is necessary with an increase in bypass ratio. Variable flow-path geometry may be required for low fan pressure ratio engines to account for operating disparities between fan flow conditions at different flight speeds [27]. A decrease in fan mass flow rate, an increase in fan rotational speed, or both, can lead to flow reversal or surge. Surge represents the upper limit of stable operation and involves the complete breakdown of continuous, steady flow in a compressor. At the same time the adoption of a VAN brings also to a noise reduction [14] and is the main focus of this study.

1.3.2 Trajectory optimization

Trajectory optimisation is another factor that can reduce aircraft noise, particularly at airports close to cities. Numerous studies have been carried out on both approach and departure procedures, as

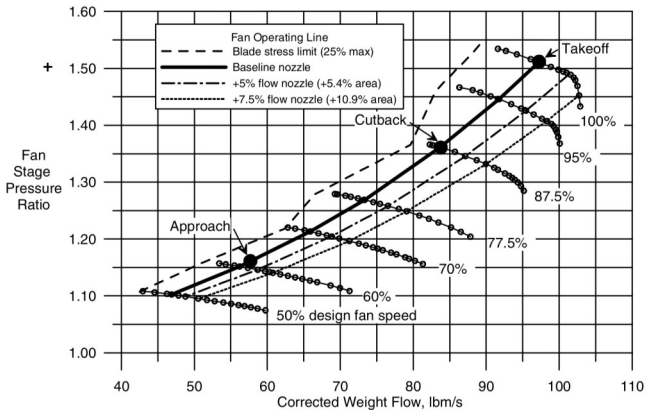

Figure 1.8: Operating line for different nozzle area openings [4]

described in [28] and [29]. It has already been mentioned in Section 1.2 how the approach phase is more standardized, having now abandoned the step descent to give space to a CDA which contributes greatly to the reduction of noise. The take-off phase is mainly determined by the aircraft manufacturer, who determines the safe speeds V1 and V2 required for take-off, but more and more airports are introducing Noise Abatement Departure Procedure (NADP). Noise abatement procedures for take-off and climb have been defined by ICAO as guidelines [30]. Basically, two procedures are defined, one that reduce noise close to the airport (NADP1) and one that reduces noise further away from the airport (NADP2). The two procedures are distinguished by a different height for flaps and slats retraction.

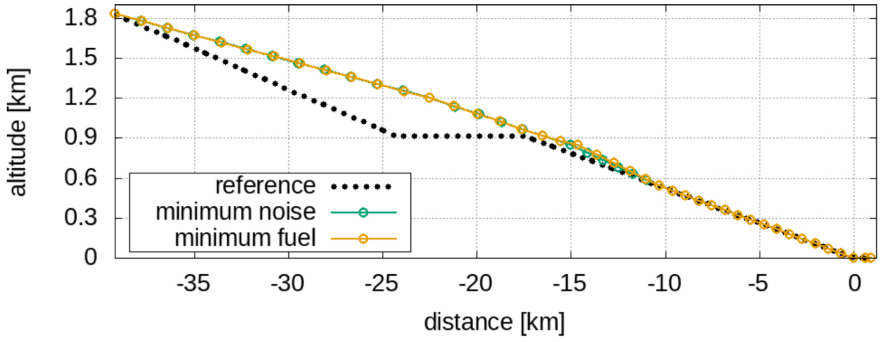

Figure 1.9: Approach manoeuvre [5]

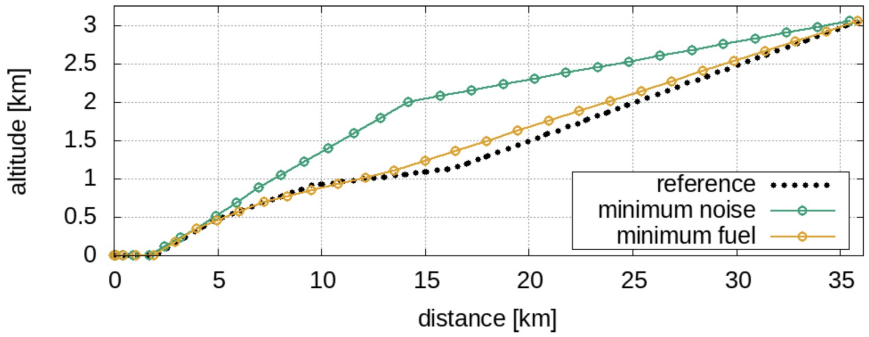

Figure 1.10: Take-off manoeuvre [5]

Figures 1.9 and 1.10 show an optimization for a twin-aisle aircraft and is provided by [5].

Although not addressed in this study, these plots remind us the multidisciplinary problem of trajectory optimization. It is in fact clear how, especially for the take-off manoeuvre the minimum noise trajectory does not correspond to the optimal fuel burn trajectory.

1.4 Computational methods for noise estimation

Aircraft noise prediction methods can generally be divided into two categories: the integrated or best practice methods and the simulation based or theoretical methods. The first are the most commonly used and are based on databases. Eurocontrol for example produces a database for aircraft noise. Although being fast and practical, these methods are limited by the applicability of data for individual aircraft and they predict the overall aircraft noise without providing information about the individual component's contribution to the total noise.

This is provided instead by the second category. The semi-empirical models which estimate the total noise by modelling and summing all the individual components at the same frequency. The most common are Aircraft Noise Prediction Program (ANOPP) [31] and Parametric Aircraft Noise Analysis Module, DLR (PANAM) [32]. ANOPP was the first computer program and integrates the flight dynamics with semi-empirical models of noise propagation and generation for individual sources. The models are rather elementary, so an update version, ANOPP2 partly uses some higher fidelity methods. More recently, the PANAM code, which focuses on comparative noise assessment for different aircraft designs. It recognises that only the dominant noise contributions count towards the total aircraft noise and therefore, it considers only the jet and the fan noise for the engine. It can also be integrated into larger simulation processes such as multidisciplinary analysis. Although the methods used are known, these tools are not publicly available. For this reason in this study the CHOICE [7] framework is used for the noise estimation of a NASA conceptual aircraft with a Ultra high bypass ratio (UHBR) installed with VAN technology.

2 METHODS

The aim of this study is to predict variations in noise source, the perceived SPL and the EPNL in order to evaluate the impact of a VAN nozzle on noise reduction. This chapter describes the CHOICE framework and the methods used to compute the input required for noise estimation.

2.1 Case study

The aircraft considered is the NASA CRM-HL, a long range wide-body concept by NASA with similar characteristics to the Boeing B777-300ER. It has become the main test case reference accessible for aerodynamic studies on commercial fleets and for the validation of adequate CFD methods. The general geometric details are shown in table 2.1, with data referring to the full scale aircraft geometry.

Parameter	Value
Cruise Mach number	0.85
Cruise altitude	37000 ft
Wing Span	58.8 m
Reference wing area	383.7 m^2
Maximum take-off mass	297500 kg
Maximum landing mass	213180 kg

Table 2.1: NASA CRM-HL

For the propulsion, a concept of a two-spool geared UHBR engine with a technology level 2030 and equipped with a VAN is being developed, to be installed in a two-engine configuration. Details of the engine are reported in table 2.2.

Parameter	Value
Fan Pressure Ratio	1.4
Bypass Ratio	16
Cruise thrust	60 kN
Take-off thrust SLS, ISA+15	420 kN

Table 2.2: Engine details - Nominal configuration

The thermodynamic cycle is given by GasTurb [33] analysis. Off-design analysis is performed using

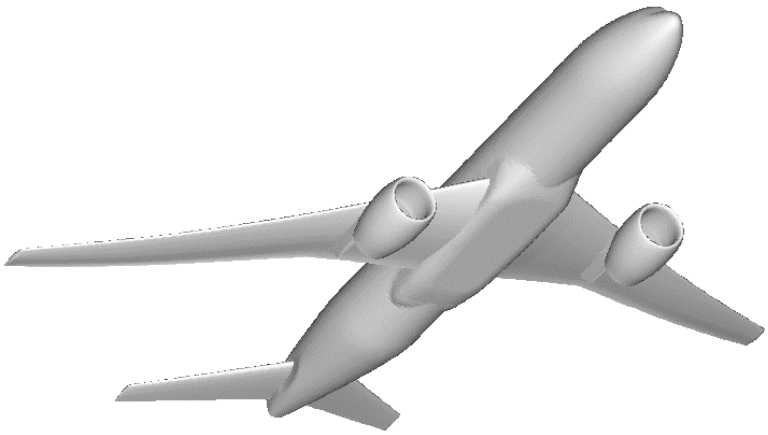

Figure 2.1: NASA CRM-HL [6]

the software to obtain the engine's cycle in the desired phases (approach, sideline and cutback). To account for the VAN effects on the engine's cycle, the entire thermodynamic state is recalculated for each jet bypass area considered.

2.2 CHOICE

CHOICE is an open source model for aircraft noise prediction model developed by the Chalmers University of Technology (Gothenburg, Sweden) [34]. It is based on empirical and semi-empirical models and it is capable of predicting the source noise level for each frequency and directivity from both individual components and the entire aircraft. It was validated by comparing the noise source estimates from specific flight trajectories with corresponding ground measurements. Specifically, the flights were performed with an A321-neo powered by the LEAP-1A engine, and it was found that it can predict the overall mean total sound intensity level to within 2 dB for all configurations. Specifically, for validation purposes, the noise source estimates were broken down according to the aircraft configuration and this was done by comparing the source noise spectra directly below the aircraft at θ=90 deg and ψ=90 deg, where θ and ψ are the longitudinal and lateral directivity, respectively. Because the aircraft was performing a normal ILS approach, a descent angle of 3 deg was used [7]. For each configuration, the mean spectra at each microphone and the overall mean are shown. This means that when the aircraft passed over a microphone with the same configuration several times, then the average of the spectra from all the passages was calculated. This approach helps to reduce the statistical variation of the noise measurements which is one of the most common problems. Noise measurements can vary even for the same aircraft type, flight procedure, and environmental conditions [35]. As a matter of fact it was demonstrated that the intensity level can vary by as much as 10 dB for the same setting.

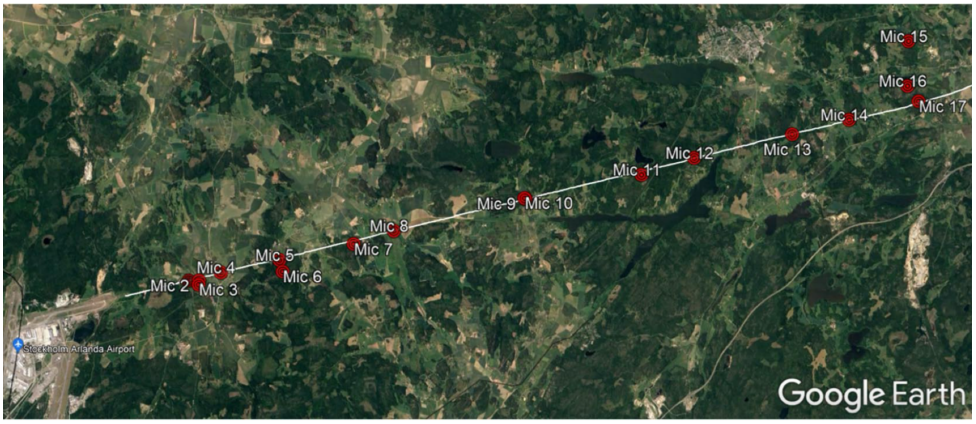

Figure 2.2: Microphone positions [7]

Figure 2.3 shows the results of the validation study, remarking how the accuracy is best at middle frequencies rather than low or high frequencies, with both the spectrum shape and the level of prediction matching the measurements. The spectra show an increase in the high frequency region, mainly driven by the fan. The prediction also shows a peak from the fan at 1 kHz, which appears as the minimum point in the data. This deviation could be due to the simplified noise suppression approximation implemented, which appears to underestimate the fan noise suppression at this frequency.

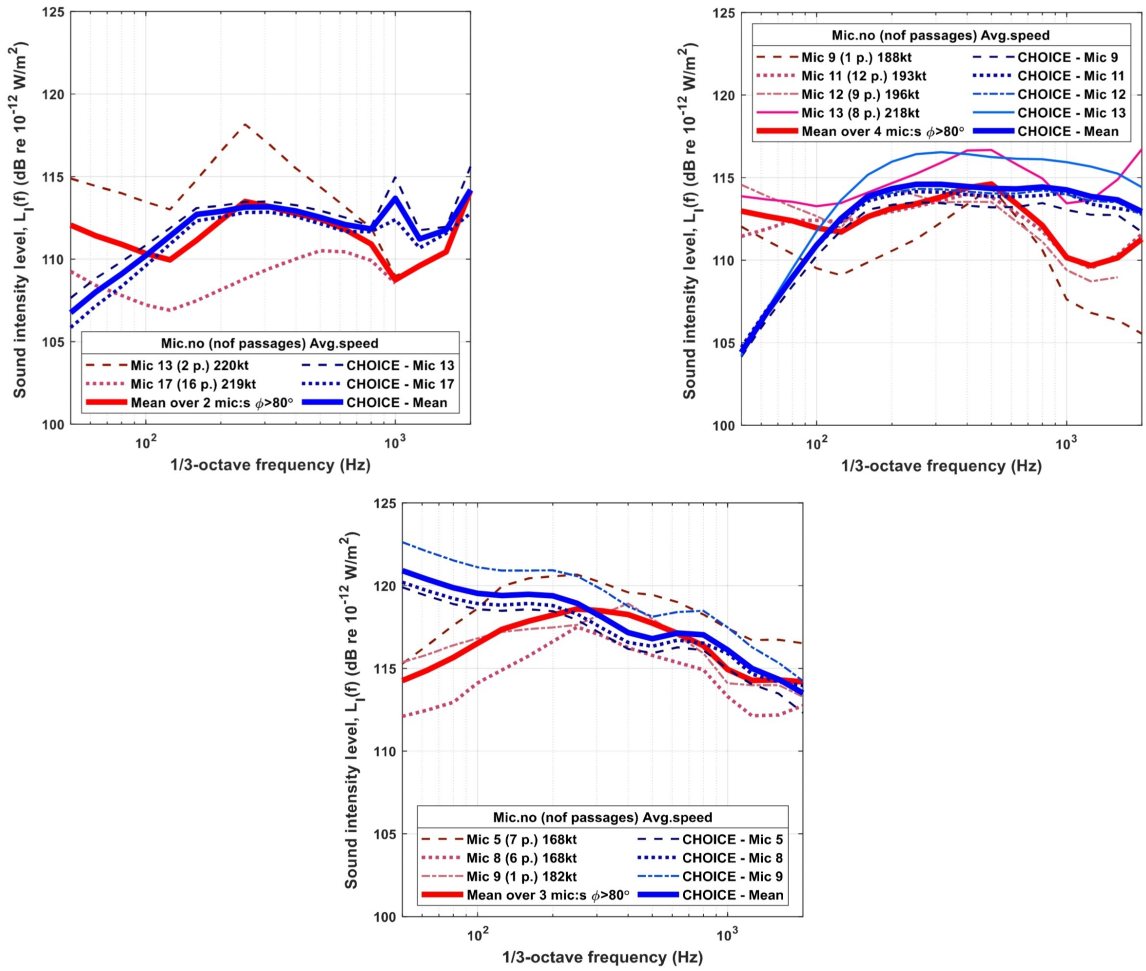

Figure 2.3: Validation for different aircraft configurations [7]

The predictions of the model are in good agreement with the measurements, particularly with respect to the noise level and the shape of the spectra in the mid-frequency region. The differences could be partly explained by the lack of geometric fidelity of the airframe components, in particular the details of the noise reduction measures, and the lack of consideration of installation effects. [7]. One of the main reasons for the occurrence of deviations is believed to be that most of the implemented noise models are quite old, and their development was based on data from older aircraft and engines. For the scope of our study, it must also be taken into account that the model was validated for the aircraft mentioned above and only for the approach phase, so that its use for a different aircraft and a different flight phase could lead to a greater difference in the results.

Figure 2.4 shows the outline of the model, starting from that, all the inputs needed are described, from the engine and airframe description, followed by the trajectory and performance data. Finally, the propagation effects are illustrated.

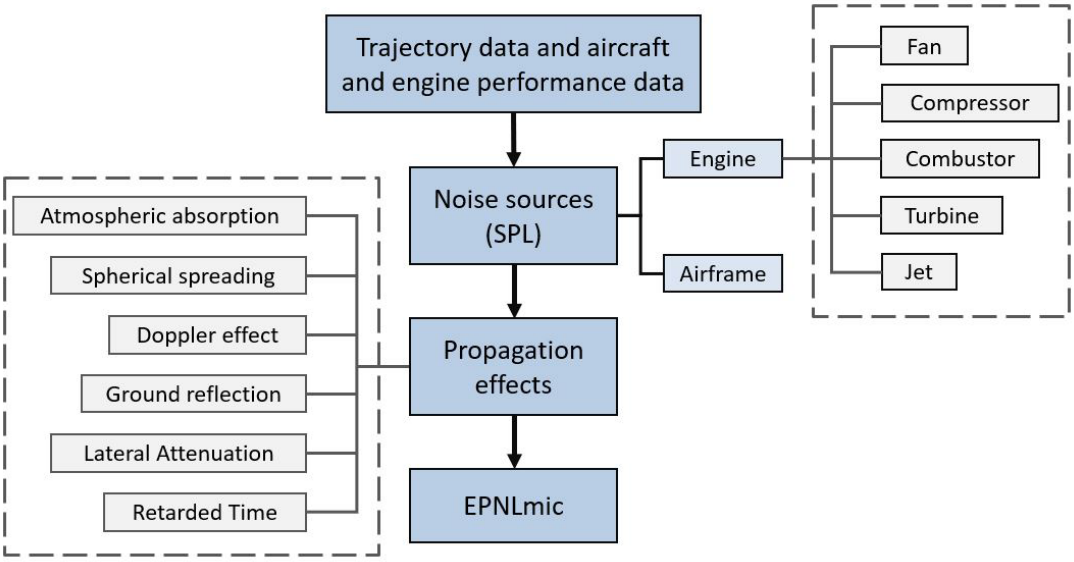

Figure 2.4: Choice model outline [7]

2.2.1 Engine modeling

The engine considered is a concept for a UHBR with a VAN. The standard configuration is considered as well as different nozzle openings, i.e. different jet bypass areas. For each variation of the bypass area, the entire thermodynamic state of the engine is recalculated considering a fixed thrust. This results in a change in the engine's operating point, allowing us to evaluate the variation in noise emissions, taking into account the effect of the VAN on the engine's state. The main focus is on the jet and fan noise, as these are the most interesting noise sources for our study, while the compressor, combustor and turbine are only modelled to obtain a complete estimate of the engine and the entire aircraft EPNL.

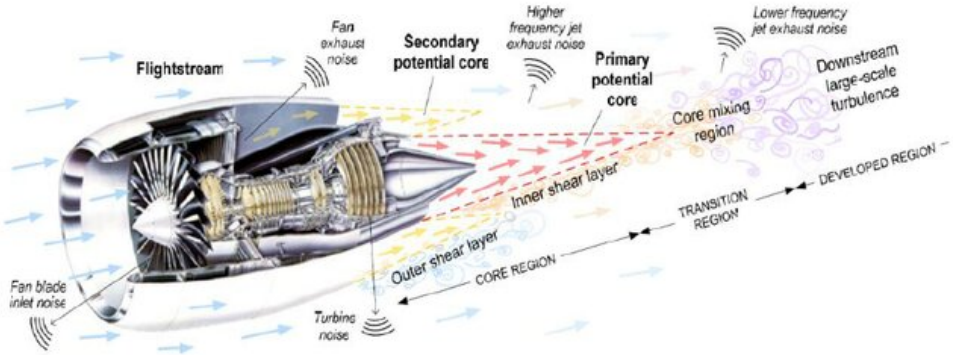

Figure 2.5: Engine noise sources [8]

Jet

Jet noise is the most studied source of aircraft noise. It is caused by the strong turbulent pulsation caused by the rapid mixing of the high-speed jet of air from the nozzle and the surrounding medium.[36].

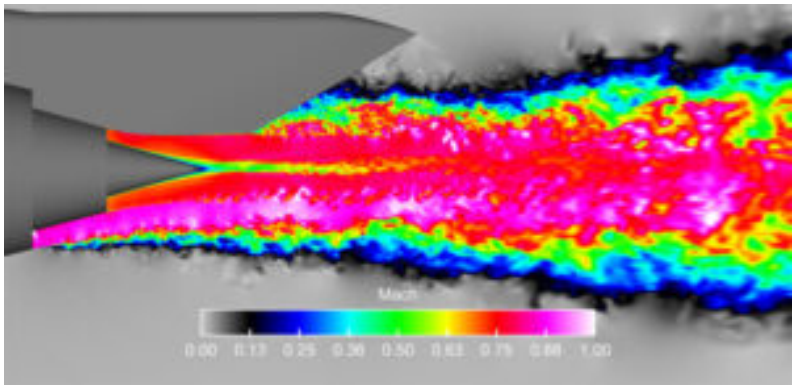

Figure 2.6: Jet turbulence [9]

In CHOICE jet noise is modelled as presented by Russell [37]. Jet noise is a function of frequency and direction and it is expressed in terms of four components: overall power level, power spectrum level, overall directivity index and the relative spectrum level (the difference between the sound pressure spectrum level in a fixed direction and the sound power spectrum level). It is a semi-empirical method, so it starts with the curve fitting of the data SPL measured in tests using bicubic splines. The bicubic splines use a standard of seven frequency parameters and seven directivity angles, and the values at these points are referred to as noise level coordinates, which define the component noise levels for all frequencies and directivities through the bicubic spline function. Each noise level coordinate is a function of the jet flow state defined by five parameters:

- Equivalent jet velocity V_e
- Equivalent jet total temperature T_e
- The velocity ratio $\frac{V_{18}}{V_8}$
- The temperature ratio $\frac{T_{18}}{T_8}$
- The area ratio $\frac{A_{18}}{A_8}$

The $\frac{1}{3}$ octave band SPL is calculated as the sum of four components:

$$SPL(\theta, \eta) = \overline{OAPWL} + D(\theta) + F(\eta) + RSL(\theta, \eta) + k_1 + k_2 + k_3 \tag{2.1}$$

In the equation 2.1 $\overline{OAPWL}$ is the normalized overall power level, $D(\theta)$ is the directivity index and $RSL(\theta, \eta)$ is the relative spectrum level. k_1, k_2, k_3 are constants depending on the jet size, microphone distance, ambient conditions and the power level and mean square pressure level reference, and their values are reported in [37]. η is the frequency parameter and is defined as:

$$\eta = 10 \log \left(\frac{f \cdot D_e}{V_e} \right) \tag{2.2}$$

where D_e is the equivalent diameter and V_e is the nozzle exit equivalent flow velocity. The four components in the equation 2.1 are defined empirically at each coordinate point and are calculated by summing their derivative values and multiplying them by the derivative multipliers given in the corresponding tables in [37]. Due to the limitations of the tests, the method is restricted to subsonic jets in a certain range of velocities and temperatures, and it has been verified that our case falls within the available range.

Fan

The model used for fan and compressor noise prediction is based on the method introduced by Heidmann [38] and subsequently improved by Kontos et al. [39]. The predicted noise is presented in 1/3 octave band frequencies of the free field noise pattern. For both the fan and the compressor inlet, this noise pattern includes broadband, discrete tone, and combination tone noise. For the fan discharge, it consists of broadband and discrete tone noise.

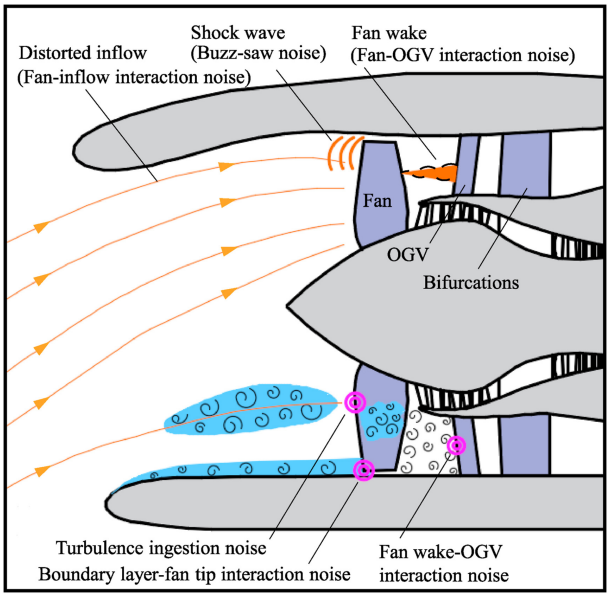

Figure 2.7: Jet turbulence [10]

Several parameters are required to predict the basic noise spectrum levels. These include the mass flow rate, the total temperature rise for a fan or compressor stage, and the design and operating point

values of the rotor tip relative inlet Mach number. Broadband noise is typically associated with the random unsteadiness or turbulence present in the flow passing the blade. This unsteadiness can be due to turbulence from a number of sources, including the wall and blade boundary layers, blade wakes and vortices, or the free stream inlet flow. Discrete tones are observed at integer multiples of the fundamental blade passage and are caused by lift fluctuations on rotor or stator blades. The peak characteristic SPL for all noise components except the combination tone noise is given by:

$$L_c = 20\log\left(\frac{\Delta T}{\Delta T_0}\right) + 10\log\left(\frac{\dot{m}}{\dot{m}_0}\right) + F_1(M_{\text{trd}}, M_{\text{tr}}) + F_2(\text{RSS}) + F_3(\theta) \tag{2.3}$$

In the equation 2.3 the first two terms include the normalised temperature ratio and the normalised mass low rate, while the last three which are function of the rotor tip relative inlet Mach number at the design point and the operating point, are taken from the graphs in [38] and [39] and vary for each component.

The sound pressure level spectrum for the inlet broadband and discharge broadband and discrete tone noise is obtained from:

$$\text{SPL}(f) = L_c + F_4\left(\frac{f}{f_b}\right) \tag{2.4}$$

while for inlet discrete tone noise:

$$\text{SPL}(f) = L_c + 10\log\left(10^{0.1F4\left(\frac{f}{f_b}\right)} + 10^{0.1F5\left(\frac{f}{f_b}\right)}\right) \tag{2.5}$$

where F_4 and F_5 are represented by functions provided in the reports and they differ for each component.

For the combination tone noise we have:

$$L_c = 20\log\left(\frac{\Delta T}{\Delta T_0}\right) + 10\log\left(\frac{\dot{m}}{\dot{m}_0}\right) + F_1(M_{\text{tr}}) + F_2(\theta) + C \tag{2.6}$$

where C equals -5 dB for a fan with Inlet guide vanes (IGV) and 0 dB without. The total combination tone noise sound pressure level spectrum is then obtained by summing the spectrum of each of the three components on an energy basis.

Combustor

The core noise model is based on the model presented by Gliebe et al. [40]. In particular we consider a dual-annular combustor. For this configuration, peaks are found at 160 Hz and 500 Hz at 130 $\deg$, taking into account the combustor geometry, cycle conditions, spectral content and directivity.

Turbine

The method implemented for turbine noise is described by Dunn and Peart [41]. It includes broadband and discrete tone noise components, which are correlated with the relative tip velocity of the last stage, the primary mass flow, and the local speed of sound at the turbine exit. In addition, the discrete tone noise is influenced by the Rotor stator spacing (RSS). The spectra of both components are normalised with respect to the fundamental blade passage frequency of the last stage of the turbine.

2.2.2 Airframe

For airframe noise different models are used to predict trailing-edge noise and landing gear noise and are described in [11].

2.2.3 Propagation effects

The noise received by a microphone or an observer on the ground is affected by various propagation and attenuation effects:

- Lateral attenuation: is the difference between the sound level at a point below the aircraft and at a point to the side. It takes into account engine installation effects, ground surface absorption and refraction, and scattering due to meteorological effects.

- Ground reflection: takes into account the sound waves reflected off the ground before reaching the microphone, which can increase or decrease sound intensity.

- Doppler effect: computes the shifted frequency from the one emitted by the moving source.

- Spherical spreading: it considers the phenomenon of uniform wave propagation away from a point source in all directions.

- Atmospheric absorption: takes into account the magnitude decrease of the wave due to classical absorption and molecular absorption.

2.2.4 Noise suppression

When predicting fan and turbine noise, as explained in the previous sections, there is a slight tendency to overestimate the noise level. This is because both methods assume a 'hard-wall' scenario, not considering any acoustic treatment.

Another reason for this overestimation is that the methods were developed based on older engine models, and they do not take into account modern noise reduction techniques. As technology advances, the impact of acoustic treatment becomes more significant, and it is essential to update these methods to reflect the advances in engine technology. For this reason, noise suppression factors are added in the code as suggested by [7].

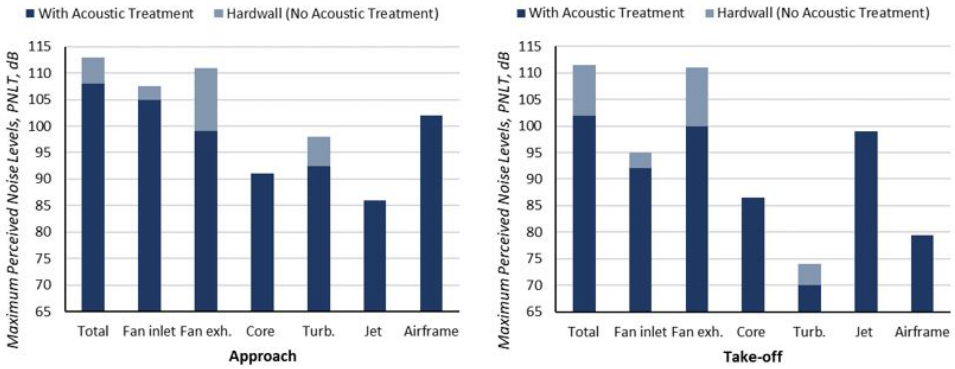

Figure 2.8: Acoustic treatment effects [11]

2.3 Input quantities

As described in the previous paragraphs, CHOICE requires several input files for the noise calculation. The various input files required are presented below, together with a description of how the parameters were obtained.

2.3.1 WeightAircraft

This file contains the engine sizing data. It is useful remember that we are studying a concept for a UHBR engine with a VAN. The engine geometry was modelled using the GasTurb software, which includes a preliminary geometry module given the engine input data. These data include all the information for the different noise models explained in 2.2 and are listed below for each component:

- **Fan, compressor and turbine:** The gearbox ratio, fan diameter and annulus area are known from the engine design, as is the fan rotation speed at design point. The relative tip Mach numbers of the fan, LPC and LPT are computed given the engine thermodynamic details. The number of stages are given by GasTurb (1 for the fan and 3 for the LPC) as is the LPC radius. The hydraulic radius is then calculated from its definition. As the engine geometry is not yet available other parameters have to be estimated by comparison with similar engines, namely the rotor stator spacing parameter for both fan and compressor and the number of rotor and stator blades for the LPC.

- **Combustor:** Only the thermodynamic state of the combustor is known so a Dual annular combustor (DAC) type is used with the same characteristics as that used on the Boeing 777-300ER, specifically on the GE90-115b engine, while the combustor exit and exhaust nozzle areas are provided by GasTurb along with the combustor nominal length and annulus height at the combustor exit.

- **Nozzle area:** The core nozzle area is given and fixed for all the configurations while the bypass area is varied from 90% to 120% of its value.

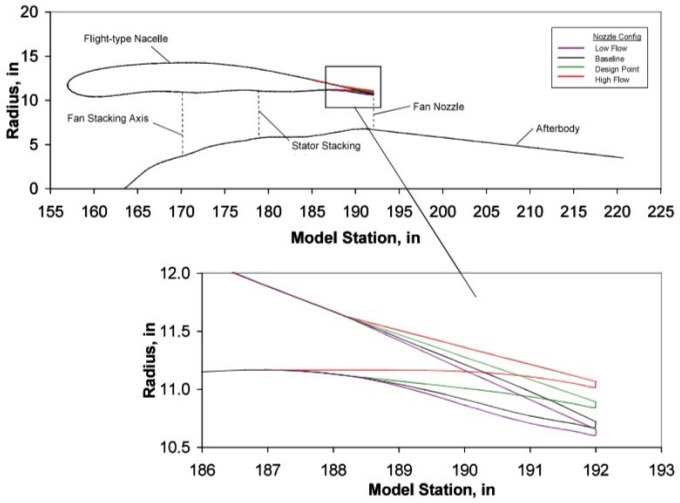

Figure 2.9: Variable bypass area [12]

2.3.2 NoiseInput and trajectory

This file defines the noise study cases. The certification point, i.e. approach, cutback or sideline, must be specified together with the microphone positions, which are given in the table 2.3.

Certification point	x (m)	h (m)	z (m)
Approach	-2000	1.2	0
Sideline	2000	1.2	450
Cutback	6500	1.2	0

Table 2.3: Microphone positions

In particular, for the sideline point several y-positions of the microphone are considered, and the loudest one is chosen, according to the certification documents [20].

All available propagation effects have been taken into account, such as ground reflection, spherical spreading, atmospheric attenuation as described in 2.2.3, also a suppression factor of 15 dB is used for the fan discharge and LPT and one of 10 dB for the fan inlet as suggested by [7], while distortion at the fan is not considered. The CHOICE Python code is divided into different modules, so first the jet module is considered, then all the others are added, i.e. fan, combustor and turbine. Since CHOICE calculations always include the airframe, this step required modifications to the code to obtain the desired quantities. Later, also the airframe module is also characterised. The aircraft considered in the study is the NASA CRM-HL, a common research NASA program [42]. A summary of the required geometric parameters of the aircraft is given below:

Component	Value	Component	Value
Wing area	383.7 [m^2]	Wing span	58.8 [m]
Horizontal tail area	78.46 [m^2]	Horizontal tail span	21.68 [m]
Vertical tail area	114.88 [m^2]	Vertical tail span	11.64 [m]
Number of flaps	4	Flap type	double-slotted
Flap area	16.65 (outer) 15.42 (inner) [m^2]	Flap span	29.72 (outer) 9.81 (inner) [m]

Table 2.4: Airframe description

The landing gear used is that of the B777-300ER, as detailed in [43] and 2.5.

Component	Value	Component	Value
Number of landing gears	3	Wheel diameter	1.3208 [m]
Strut diameter	0.18 [m]	Wire or hydraulic pipe diameter	0.0254 [m]
Number of wheels	2, 6, 6	Number of main struts	1

Table 2.5: Description of landing gear components

Other parameters have to be modified depending on the certification phase being analysed, since the aircraft configuration changes during these phases . These are the flap and slat deflections and the landing gear position, as shown in the table 2.6.

Certification point	Flap deflection	Slat deflection	Landing gear
Approach	0.523598 [rad]	0.383972 [rad]	Extended
Sideline	0.261799 [rad]	0.383972 [rad]	Extended
Cutback	0[rad]	0 [rad]	Retracted

Table 2.6: Certification points aircraft configurations [19]

2.3.3 Performance data and trajectory

Finally, the performance data are required. These include the engine operating parameters and can be specified for each point on the flight path. A file is required for each module. For the airframe performance, the angle of rotation θ in radians is requested together with the flap and slat deflections (described in 2.6) and the landing gear position (0 for retracted, 1 for extended) where the rotation angle

θ is found by:

$$\theta = \alpha + \gamma \tag{2.7}$$

where α is the angle of attack and γ is the climb/descent angle. For the coaxial jet performance, the mass flows of both the bypass and the core nozzle are required, as well as for the velocities and the total temperature at the two stations. The combustor file requires the total pressure and temperature of both the inlet and outlet, together with the mass flow. The fan noise is described by the M_{tr} and M_{trd}, here referred to as $Mtip_{fan}$ and Mu_{fan}, then the rotational speed in rounds per second, the ΔT across the fan stage and the mass flow. The LPC performance file requires the same information as the fan with the only exception that the ΔT required is that across only one stage. Finally the turbine parameters are required. These are the velocity relative tip speed of the last rotor, the turbine exhaust temperature, the rotational speed, the mass flow and the axial velocity. The mass flows, total temperatures and pressures were known from GasTurb, but further calculations had to be made in order to find the speeds and Mach numbers required at different stages. These were found once the geometry of the engine and the areas of the various stations had been defined.

Trajectory definition

In order to have a proper prediction of the EPNL, a trajectory for the approach and take-off is needed. The different phases are now analysed. In order to take into account the whole aircraft, all values given here refer to the full configuration, i.e. geometry data refer to the full span aircraft and two engines are considered for thrust.

Approach: For the approach phase, according to regulations [44] and common approaches, a CDA is chosen with a descent angle of $3\,\text{deg}$. As only one operating point of the engine is known, the True Air Speed (TAS) is kept constant along the trajectory and is calculated knowing the Mach number and the speed of sound, for low altitudes a constant $a = 349.039 m/s$ is used, which is the speed of sound at $h = 0$ with a temperature deviation of $15\,\text{deg}$ from International Standard Atmosphere (ISA). A Python code is used to integrate the aircraft dynamic equations. Assuming a constant TAS and constant angle of descent the system of equations reduces simply to:

$$\begin{cases} sin(\gamma) = \frac{T-D}{W} \\ cos(\gamma) = \frac{L}{W} \\ V_z = TAS \cdot sin(\gamma) \end{cases} \tag{2.8}$$

where γ is the angle of descent, T is the thrust, D is the aircraft drag, L the lift force and Vz the vertical velocity. The vertical velocity can be directly computed knowing the TAS and descent angle, while the weight is already known from the [42]. For the approach phase the Maximum Landing Weight (MLW) of $213180kg$ is used. Consequently, the lift force can also be computed by inverting the second equation in (2.8). At this point T and D remain unknowns. So the C_L is found using:

$$C_L = \frac{2 \cdot L}{\rho \cdot TAS^2 \cdot S} \tag{2.9}$$

At this point the wing polars in the approach configuration are considered from [45]. To account for

tail and landing gear effects, two terms are added to the $CLvsCD$ graph as suggested by [46].

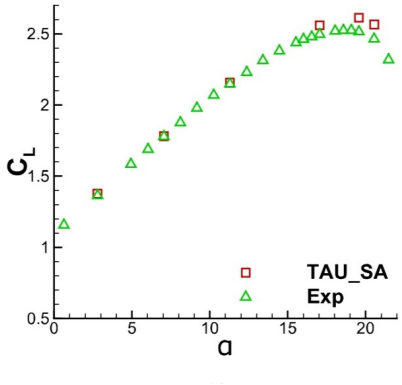

(a) Cl vs alpha - Landing [45]

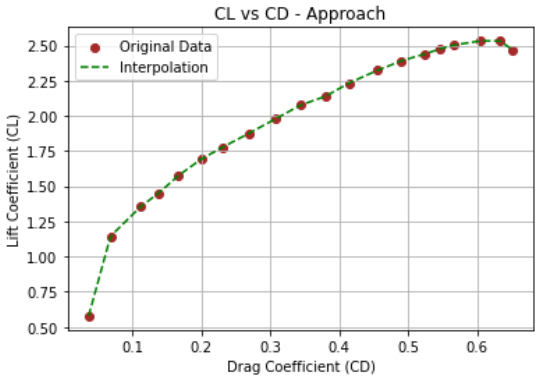

(b) Cl vs Cd - Landing

Knowing the C_L, we can now calculate the required angle of attack α and the C_D of the aircraft in landing configuration. So the total drag can be calculated using:

$$D = \frac{1}{2} \cdot \rho \cdot C_d \cdot TAS^2 \cdot S \tag{2.10}$$

T is then found from the first equation in 2.8. The results for the approach phase are now reported, together with the plot of the trajectory, including the microphone position for the certification point.

Parameter	**Value**	**Parameter**	**Value**
M	0.22	W	2090582 N
γ	-3 deg	α	7 deg
C_L	1.585	C_D	0.167
D	219629 N	L	2087716 N
T	110216 N	θ	4 deg

Table 2.7: Approach

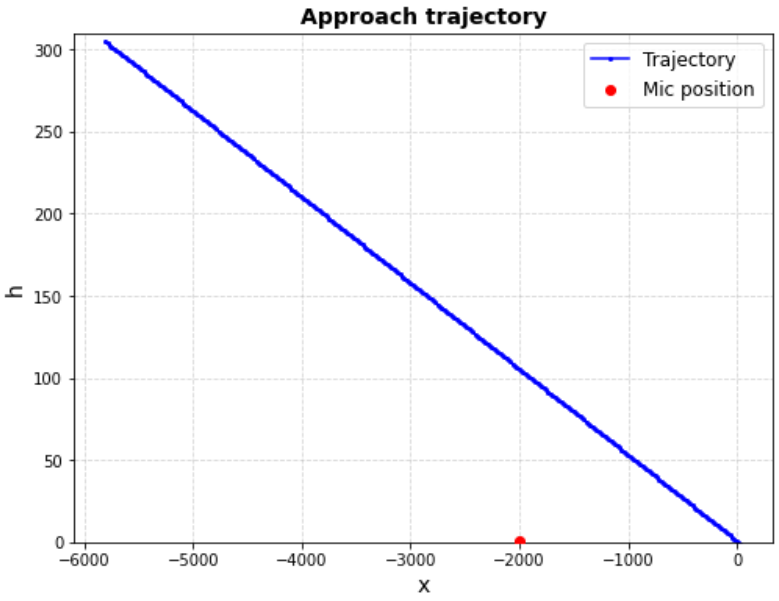

Figure 2.11: Approach trajectory

Sideline and cutback: For the take-off phase, as stated in 1.2.2, defining a preliminary angle of descent is more challenging than for the approach phase, with regulations that allow a wide range of possibilities. Since we are interested in noise reduction in the vicinity of the airport, the maximum climb gradient [47], with a cutback height of 457 m (1500 ft), is imposed. The cutback height is chosen to be the same as the one at which the aircraft switches to a clean configuration. For the two different phases, the polars of the take-off and the free air configuration have been used, and as same as done for the approach,terms for tail and landing gear (this last one only for sideline) are considered in the $CLvs.CD$. Regarding the weight, MTOW is used for the take-off, then the weight reduction due to fuel consumption has been used to estimate the weight at cutback. For the sideline phase, as mentioned earlier, the maximum climb gradient is imposed, in order to get out of the lower altitudes which cause more annoyance. The climb gradient used is 15.6% giving a Rate of Climb (ROC) of 15.24 m/s, where:

$$ROC = V_z \tag{2.11}$$

and climb gradient is given by:

$$Climbgradient = \frac{ROC}{TAS} \cdot 100[\%] \tag{2.12}$$

assuming $Groundspeed = TAS$ in absence of wind.

For cutback, the minimum certification climb gradient (i.e. 4%) is adopted, resulting in a 2.29 deg climb angle. At this point, the same steps for the approach phase are followed in order to obtain all the

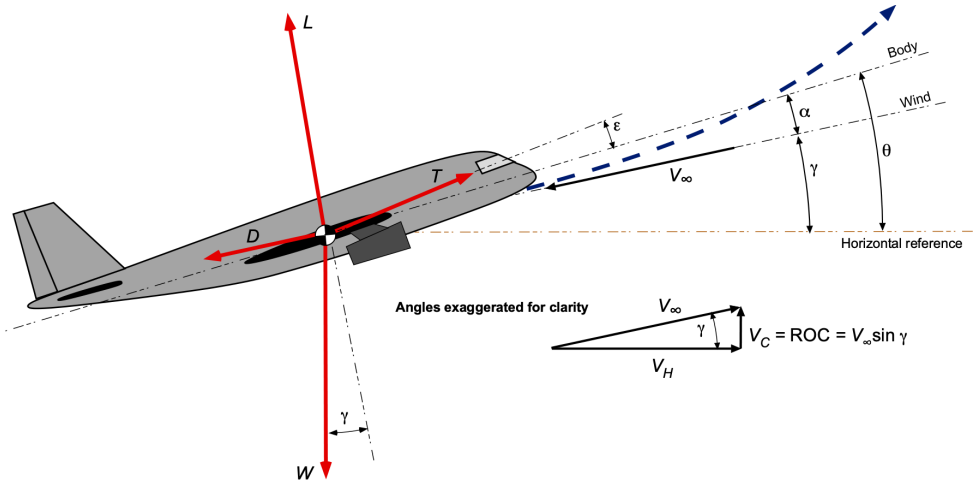

Figure 2.12: Climb [13]

required quantities for the take-off phases, which are given in tables 2.8 and 2.9.

Parameter	Value	Parameter	Value
M	0.28	W	2918475 [N]
γ	9 deg	α	5.3 deg
C_L	1.384	C_D	0.174
D	362554 [N]	L	2881788 [N]
T	817501 [N]	θ	14.3 deg

Table 2.8: Sideline

Parameter	Value	Parameter	Value
M	0.28	W	2913570 [N]
γ	2.29 deg	α	6 deg
C_L	1.426	C_D	0.115
D	236207 [N]	L	2910244 [N]
T	352710 [N]	θ	8.3 deg

Table 2.9: Cutback

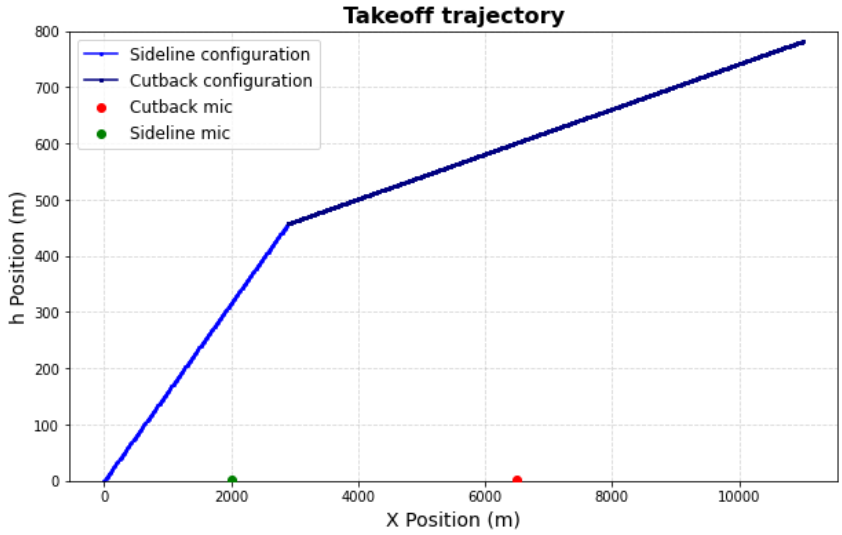

Figure 2.13: Takeoff trajectory

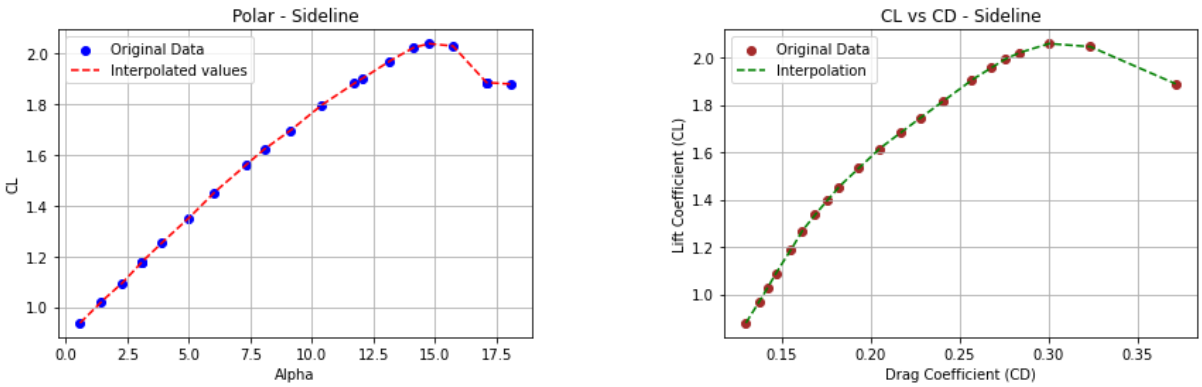

Figure 2.14: Sideline polars

3 RESULTS

This chapter presents the results of the study to quantify the effect of a VAN solution on the noise problem. The primary focus is on the jet and fan, but the results for the entire aircraft are also discussed. Comparisons with similar studies are also shown to demonstrate the reliability of the results obtained. Nine different nozzle configurations with varying bypass areas ranging from 90% to 120% are studied, thus the results only consider the nozzle openings, as they are the most relevant cases for both propulsion and noise studies [14]. The output from CHOICE is a sound pressure level matrix for each frequency and longitudinal directivity and for each point of the trajectory. This matrix is generated separately for each component, and the total noise is calculated by summing all the individual sources and the EPNL for the separate components and total aircraft is computed.

3.1 Jet noise

In 2.2 the model used for the jet noise was described. Now we focus on the parameters that have the most influence on the jet noise generation. The noise emitted by a jet with a variable area nozzle is reduced due to the lower relative jet speed and the fan pressure ratio. An estimate of the reduction in jet noise can be made based on the assumption that the jet mixing noise is proportional to the eighth power of the relative jet velocity. Based on these considerations, Michel [14] found a noise reduction of 2.6 dB during the initial climb phase when the nozzle is opened by 15% and reported in figure 3.1, by using the following equation:

$$\Delta SPL = 80\,\mathrm{dB}\lg\left(\frac{M_{j,v}-M_f}{M_{j,c}-M_f}\right) + 10\lg\alpha + 10\lg\phi + 20\lg\frac{\sigma_v}{\sigma_c} \tag{3.1}$$

whit σ the jet stretching factor:

$$\sigma = 1 + AM_f/\left(M_j - M_f\right) \tag{3.2}$$

and A was set to 1.5. In equation 3.1, $M_{j,v}$ is the jet bypass Mach number,$M_{j,c}$ the core nozzle Mach number and M_f the flight Mach. α represents the nozzle opening factor A_v/A_c and ψ the opening ratio of fully expanded jet A_j/A_v.

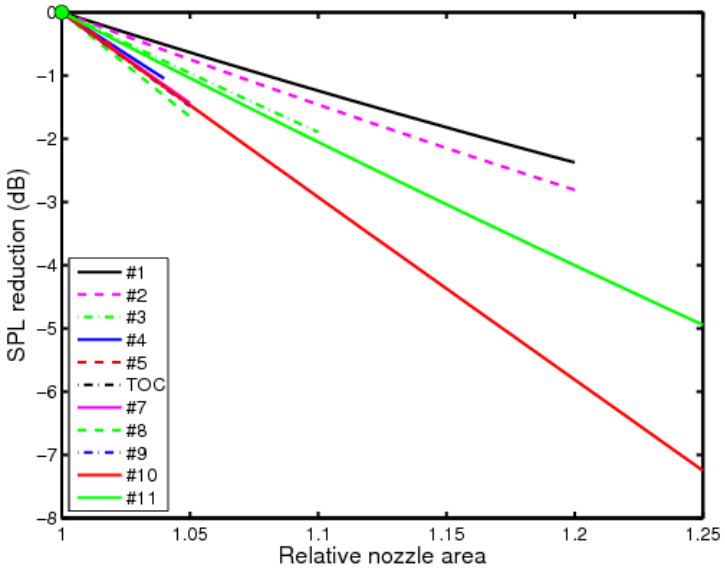

Figure 3.1: Noise jet reduction with varying nozzle area [14]

In figure 3.1, #2 represents the initial climb phase while #11 the approach phase and are the aspects of interest for our study. It can be seen how a reduction of up to almost -4 dB is predicted in the SPL in the approach phase with a nozzle opening of 20% and of almost -3 dB in the initial climb. The same formula with the data of the nozzle being considered is plotted together with the results obtained in our study for comparison and is shown below in Figure 3.2.

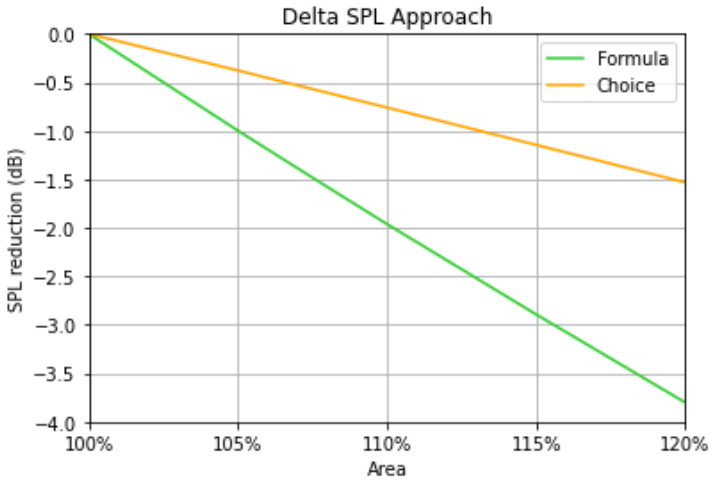

Figure 3.2: Noise jet reduction comparison

One can see that the noise reduction is smaller. However, a reduction is still noticeable and it is analysed deeper now.

3.1.1 Jet source noise

We start by analysing the noise at the source, i.e. one metre from the nozzle. This is obtained in CHOICE by back propagation of the sound waves recorded by the microphone. This allows us to consider a lossless problem, i.e. an estimate of the noise without any external factor due to the atmosphere or wave dissipation, and thus to detect the undisturbed effect of varying bypass area on the nozzle noise. The output of CHOICE is a 3D matrix for the jet source noise, so for each point on the trajectory the SPL is calculated for each directivity and frequency. We start by considering the directivity issue. In fact, a noise source does not emit equally in all directions. To show this characteristic and to find the most intense directivity, the Overall Sound Pressure Level (OASPL) is calculated for one point of each certification point. The OASPL is the equivalent SPL obtained by integrating over all the frequencies, allowing us to consider a source independently of its frequency.

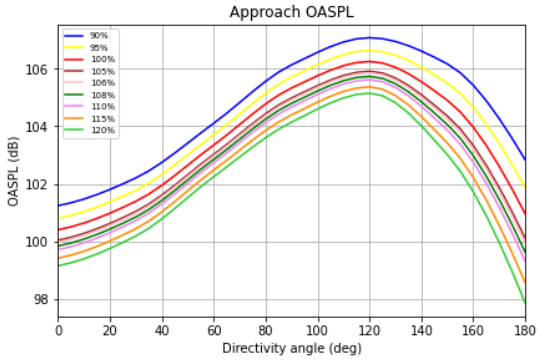

Figure 3.3: OASPL - Approach

The same can be seen using polar diagrams, as in figure 3.4.

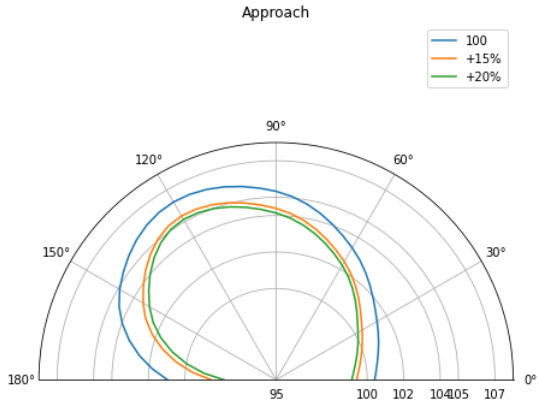

Figure 3.4: OASPL (dB) vs Directivity (deg) - Approach

For jet noise, the peak level directivity angle is usually 150 deg [37]. This is what we get for the take-off

phases, while for the approach it is around 120 deg. This can be explained by the different jet velocity ratio between the approach and the take-off phases. As a matter of fact, the core nozzle velocity and the bypass nozzle velocity strongly influence the shape of the spectrum [15]. We can also see that an opening of 20% leads to a OASPL reduction of almost 2 dB at the peak, while the reduction becomes greater at higher directivities. From [37] we also know that the standard error over all frequencies and directivity angles is 1.5 dB. For the sake of completeness, the same graphs are now shown for the take-off phases. What we have just seen is confirmed, as the peak is now at 150 deg. Similar polar diagrams are found for the B777 as shown in figure 3.7.

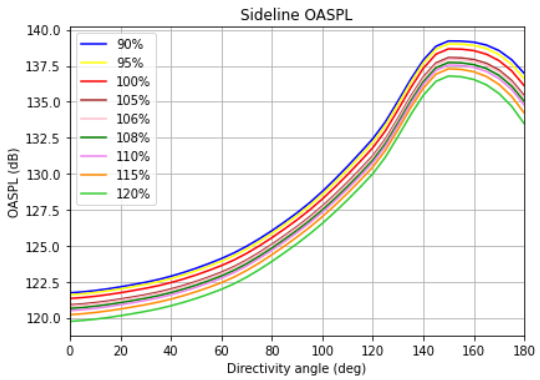

(a) OASPL - Sideline

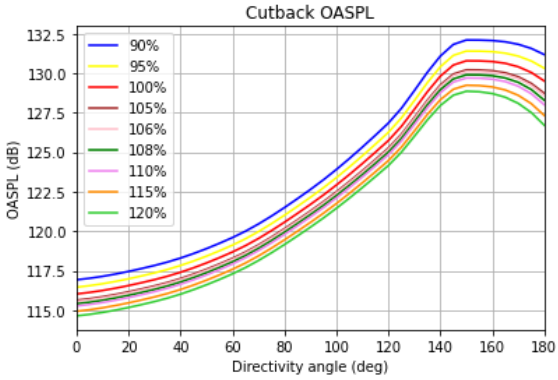

(b) OASPL - Cutback

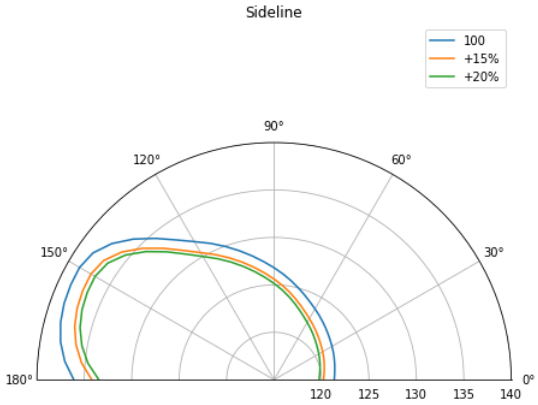

(a) OASPL (dB) vs Directivity (deg) - Sideline

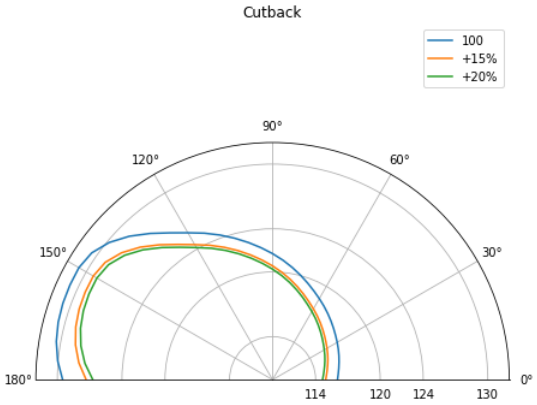

(b) OASPL (dB) vs Directivity (deg) - Cutback

As expected from the theory, the largest SPL value is obtained in the sideline phase, as the engine is operating at its maximum, resulting in a greater jet speed, which is slightly reduced by the cutback and is much smaller in the approach phase. There is also a greater reduction in the peak directivity in the sideline phase. This confirms that the jet noise is more pronounced in the take-off phase, while other noise sources dominate in the approach phase.

We proceed with the analysis of the source frequency spectrum. We have already seen that the

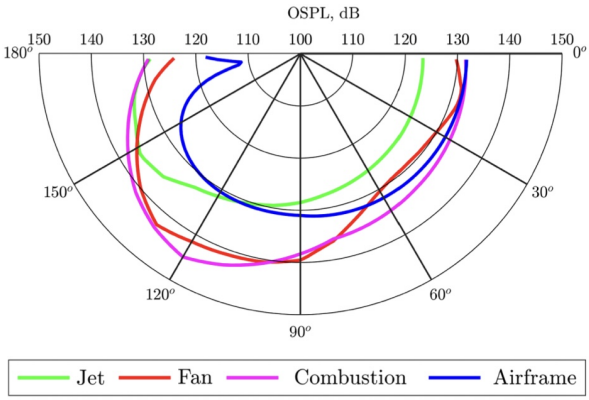

Figure 3.7: B777 takeoff OASPL [15]

emission of a noise source is not the same at all directivity angles, so it is important to find the directivity that reaches the microphone. CHOICE gives the possibility to find the angle for each point of the trajectory. This angle will change throughout the trajectory, so we will only plot the loudest directivity for the three phases.

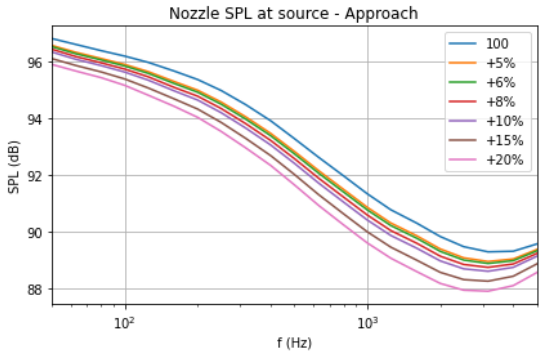

Figure 3.8: Jet source at approach, $\theta = 120\,\mathrm{deg}$

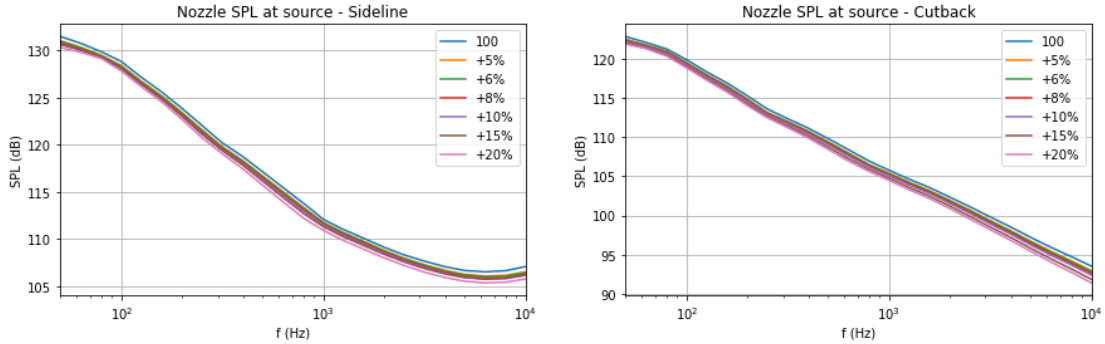

(a) Jet source at sideline, $\theta = 150\,\mathrm{deg}$

(b) Jet source at cutback, $\theta = 150\,\mathrm{deg}$

Again, the effect of opening up the bypass area is noticeable, with a reduction of almost 2 dB SPL at all frequencies.

Similar results can be seen for the take-off phases. The mean SPL reduction in the three phases is shown in figure 3.10, where it can be seen that the reduction is similar in all cases, with a slightly greater reduction obtained for the cutback, where a reduction of 1.4 dB is obtained for a nozzle opening of 20%.

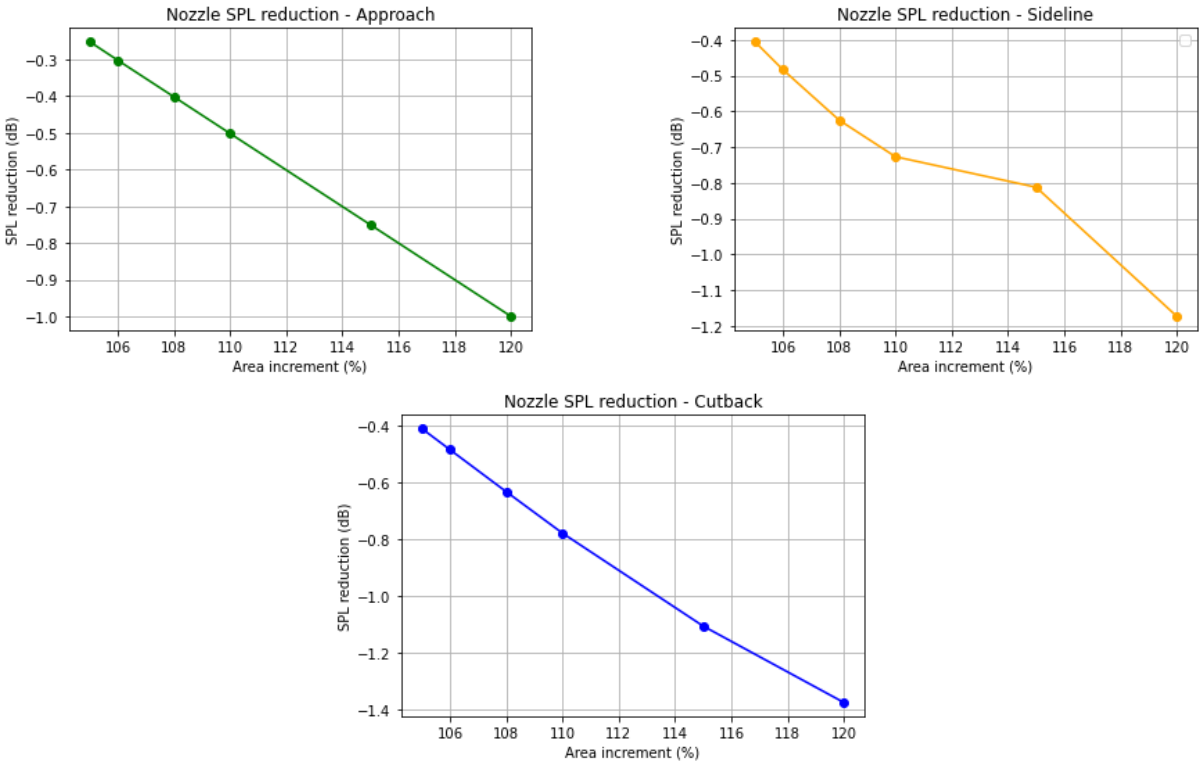

Figure 3.10: Source jet noise reduction

The results can be compared with [16], which gives several different configurations and distances from the source. Here the closest case for a similar nozzle is shown in figure 3.11, where the dots represent experimental data and the line the results from the Stone model for jet noise, which is one of several

semi-empirical methods available. It can be seen that the trend of the plots is similar to the experimental data, with the highest values at the lowest frequencies. The slight increase in SPL at approach and sideline can be explained by the lower accuracy of the model at the highest frequencies.

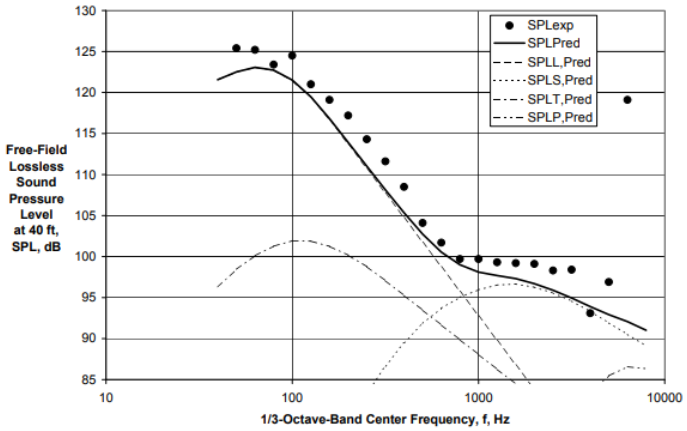

Figure 3.11: Nozzle SPL, $M_f = 0.28$ [16]

3.1.2 Perceived Jet Noise

Our aim is to evaluate the SPL perceived by an observer on the ground, therefore the perceived SPL is now analyzed.

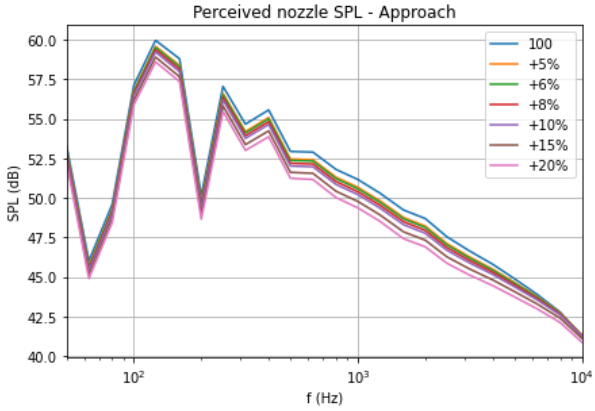

Figure 3.12: Perceived SPL - Approach

The moment when the aircraft is directly over the microphone is considered, as the code has been validated under these conditions and it represents one of the loudest measurements. This implies that the directivity reaching the microphone at that time is the one being measured. Differently from the source, some peaks are now present due to propagation effects 2.2.3. In particular, these peaks occur at the lower frequencies (around 100-200 Hz) finding good agreement with the theory [15], then a continuous SPL reduction is found. The reasons for this are, as stated in 3.1.1, that the highest SPLs for the nozzle are found at the lower frequencies and that the low frequency sound is less absorbed by the atmosphere [17].

By analyzing the measurements provided by [15] for the B777, a similar shape of the noise spectrum is found in the low frequency range. These measurements refer to a take-off phase, meaning that the jet source is dominant at least in the low frequency range.

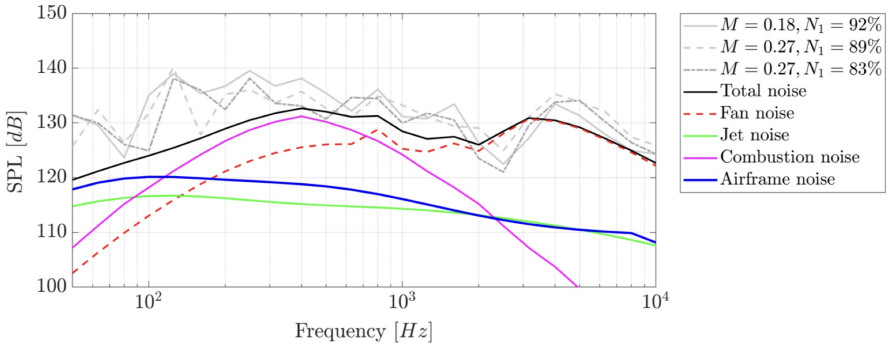

Figure 3.13: B777 takeoff noise measurements [15]

Comparing the results of the study presented in figure 3.15 with 3.14 the reductions found are less than expected from the theory, but follow the same trend. For completeness, figure 3.15 also shows the OASPL values for 90% and 95% of the bypass area, which results in a higher value as already mentioned. This is not too worrying as the nozzle would only be closed at the top of the climb, where noise is not the main concern [14].

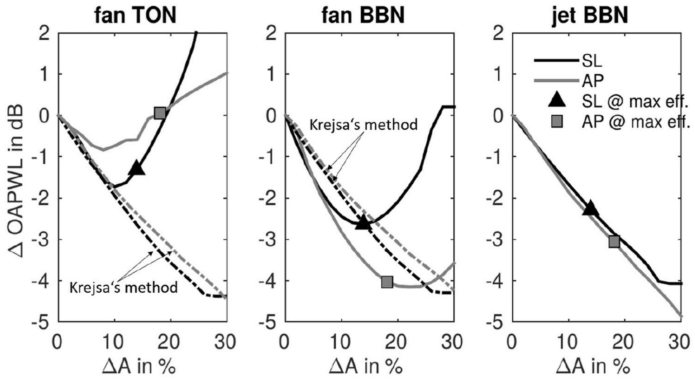

Figure 3.14: OAPWL reduction [17]

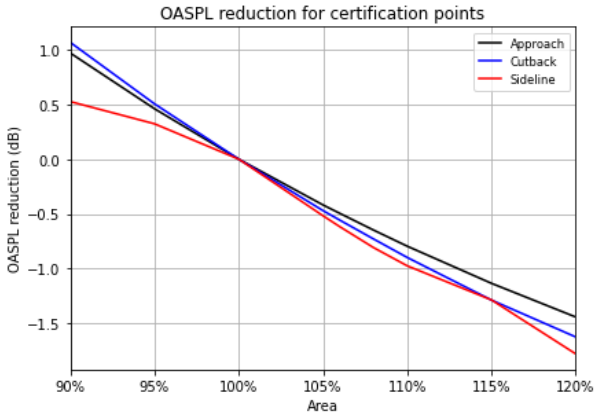

Figure 3.15: OASPL reduction - jet

In summary, jet noise is steadily reduced as the nozzle is opened, in fact, considering a constant thrust, the increase in mass flow must be compensated by a reduction in the fan pressure ratio, thus resulting in a lower jet exhaust and therefore to a weaker source of jet noise. Apart from the nozzle, Moreau [17] also conducted a fan noise study which, as we will be analyzed in the next paragraph, is not as straightforward as the jet noise.

3.2 Fan noise

A similar analysis is now performed for the fan noise. It was already introduced in 2.2.1 how the fan generation mechanism is composed of five different sources. At subsonic fan tip speeds the tones occur at harmonics of the blade passage frequency, while for supersonic tip speeds the tones are at multiples of 1/rev. At subsonic tip speeds, fan tones can be generated by inlet flow distortions and by blade and exit guide vanes interactions [48]. At supersonic tip speeds, the combination tone noise is experienced in addition to the other two sources. It results from shock waves at the leading edge of the rotor blades. Furthermore, it is generated at 1/rev and propagate only out of the engine inlet. We start by considering Figure 3.14 where it can be seen that, unlike the jet, the fan noise reduction is not linear with the bypass opening. The solid lines show an analytical method developed by Moreau while the dashed lines show an empirical approach developed by Krejsa. Beyond the optimum point, the analytical model shows an increase in noise due to the increase in wake size. The tonal noise of the fan is less reduced and may be even greater than in the design when the nozzle is opened.

3.2.1 Fan source noise

Following the same approach as for the jet, the fan noise source is now analysed. The loudest directivity reaching the microphone is chosen. The spectra for the fan inlet and discharge are reported for the three certification points. The method proposed by [38] and then improved by [39] describes the spectrum content, spectrum levels and corrections for particular operating conditions and directivities. In particular the spectrum content is characterised by a log-normal distribution function with a centre frequency of 2.5

times the blade passage frequency.

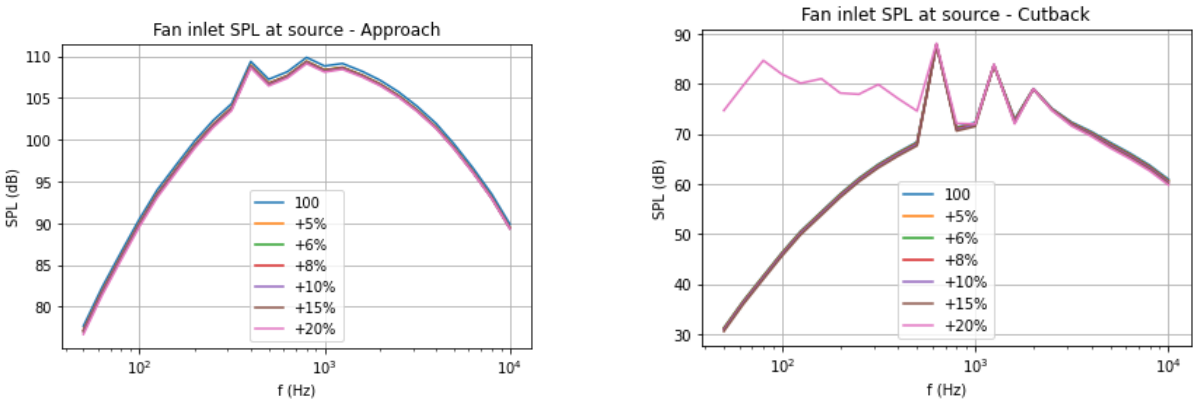

(a) Fan Inlet - Approach, $\theta = 30\,\mathrm{deg}$

(b) Fan Inlet - Cutback, $\theta = 125\,\mathrm{deg}$

Figure 3.16: Source Fan Inlet SPL

If we compare the results obtained for the approach and cutback points, we can see the following:

- The fan noise is relevant in all flight phases, in fact higher SPL values are found for the approach phase.
- As expected the peak in the cutback phase moves to the higher frequencies as the fan rotates faster.
- The peaks are more pronounced for the cutback phase.
- With a 20% area opening the fan tip Mach number becomes supersonic, which explains the different shape for the last configuration in Figure 3.16b.

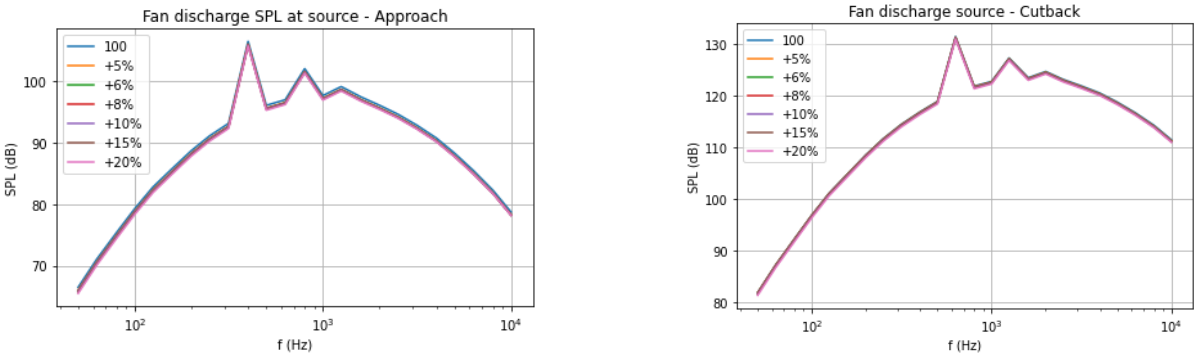

(a) Fan Discharge - Approach, $\theta = 30\,\mathrm{deg}$

(b) Fan Discharge - Cutback, $\theta = 125\,\mathrm{deg}$

Figure 3.17: Source Fan Discharge SPL

For a better understanding of the noise reduction, the mean difference for both the fan inlet and discharge at all frequencies is calculated and is now shown for the three points. Starting from the

approach point it can be seen that the reduction for both fan inlet and fan discharge is linear with the nozzle opening.

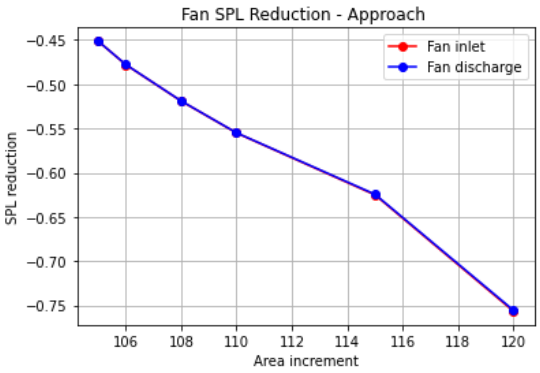

Figure 3.18: Fan SPL reduction - Approach

However, on the take-off phases, the behaviour is different and this is due to the addition of the combination tone noise, which results in an increase in the fan inlet SPL. We have already seen that at cutback only an opening of 20% gives a supersonic fan tip Mach number, while at sideline it is always greater than 1. Therefore, at cutback, the SPL increase is confirmed with the last configuration and at sideline, the SPL value is greater for small openings and decreases with further openings of the nozzle.

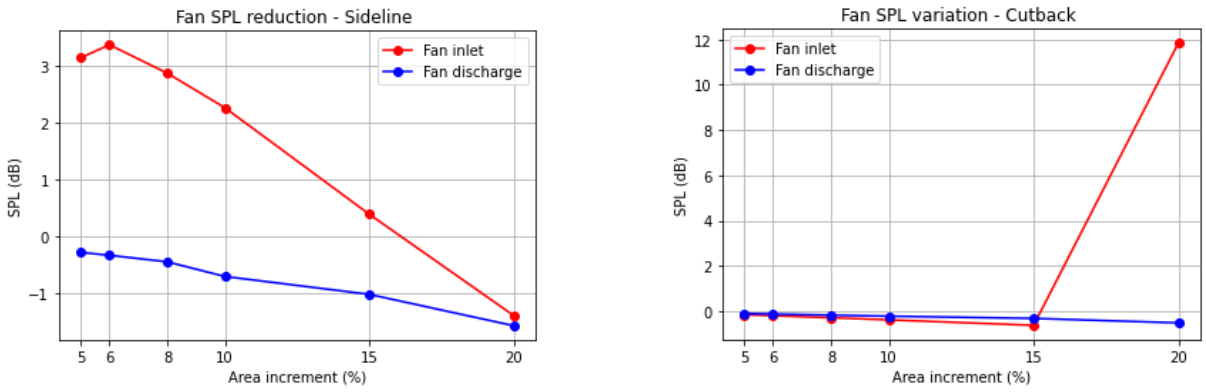

Figure 3.19: Source fan noise variation

3.2.2 Perceived Fan Noise

For a better overview, the SPL at the microphone position are summed to obtain the total fan noise. The perceived noise SPL at the points above the microphone shows a similar trend to the source noise, but scaled by propagation and atmospheric attenuation effects, so only the fan noise at approach is shown here.

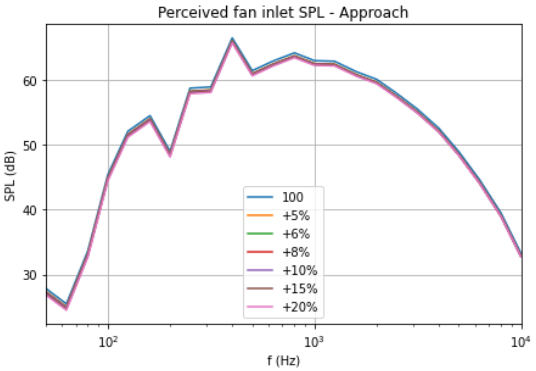

(a) Fan Inlet SPL

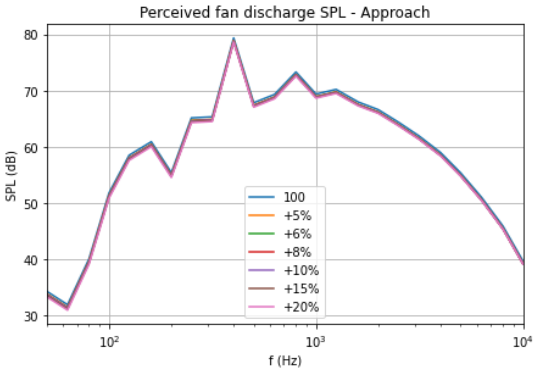

(b) Fan Discharge SPL

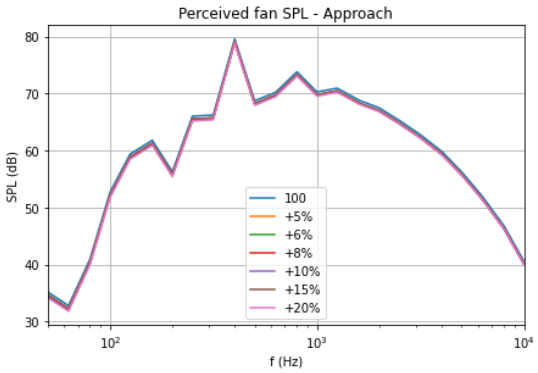

(c) Total fan SPL

Figure 3.20: Perceived fan SPL

3.3 Total aircraft noise and EPNL evaluation

3.3.1 Airframe noise

In order to obtain an accurate estimate of the EPNL for the three certification points, the airframe must be considered in addition to engine noise. Progress made in this field showed that the two main noise sources responsible for airframe noise are the high-lift systems and the landing gear [22]. Specifically, high-lift systems noise sources include: 1. trailing edge noise; 2. flap edge noise; 3. leading edge noise. The currently available methods often lack the geometrical details, which are often unknown, and since they are based on empirical evidence, the results are limited. Also, regarding landing gear noise, only

empirical methods are available.

Taking into account the configurations for the three points described in 2.3.2, the following EPNL values are obtained for the airframe:

Certification point	**EPNL dB**
Approach	95
Sideline	83
Cutback	71

Table 3.1: Airframe EPNL

From table 3.1 one can notice the sensitivity of the code to high-lift systems and landing gear. In fact, on approach we had the highest values of angle of deflection angles for both flaps and slats and landing gear extracted. Their deflections were reduced for sideline with the landing gear still extracted. Finally, for cutback, a clean configuration was considered, i.e. no deflections for flaps and slats, and the landing gear was retracted. This resulted in a difference of 14 dB between the different configurations.

3.3.2 EPNL evaluations

This section examines the EPNL values obtained from the study, both for the individual noise sources and for the aircraft as a whole. The EPNL results are consistent with the SPL results.

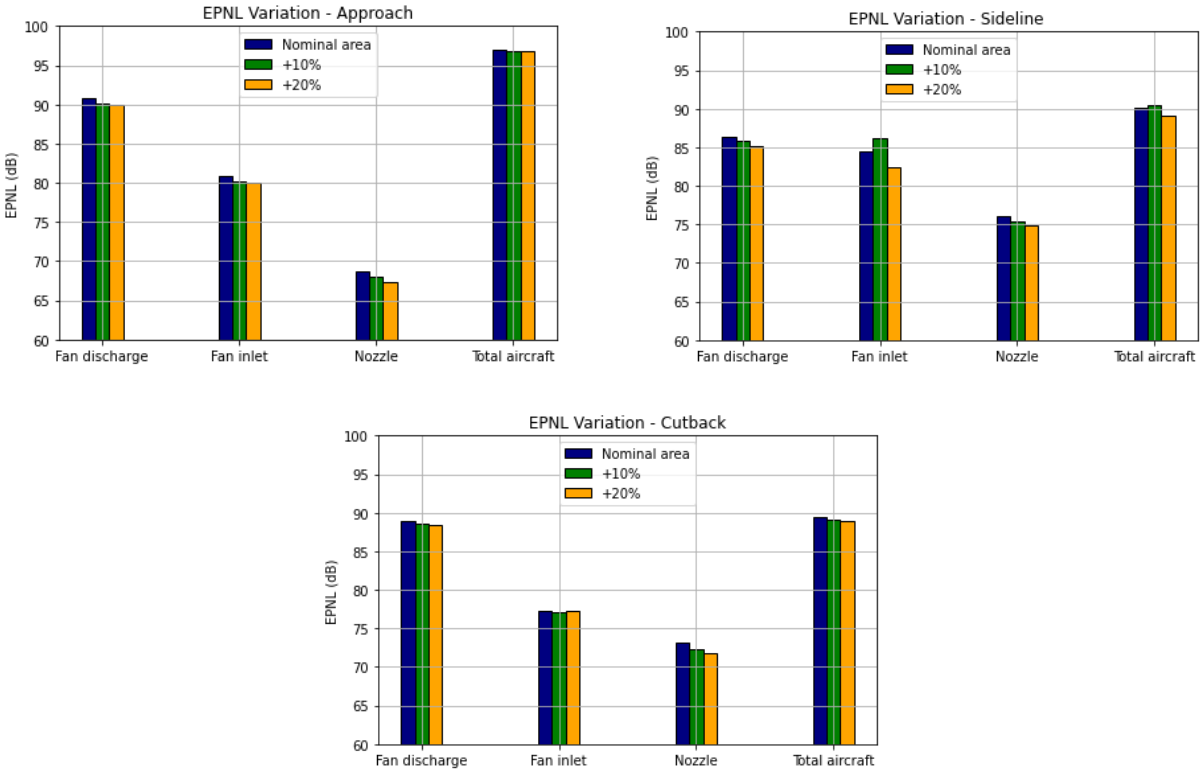

Figure 3.21: EPNL

Figure 3.21 shows how the EPNL is always reduced with nozzle opening for approach and cutback, for all noise components, resulting in a total aircraft noise reduction. Although the largest reductions for the engine noise sources are found for the approach phase, the resulting total aircraft noise is not affected due to the high airframe contribution as seen in 3.1.

The same plot is also shown for the sideline point, where it can be seen that for a 10% area opening there is an increase in the fan discharge noise. The EPNL variations for the different nozzle geometries are analysed in more detail.

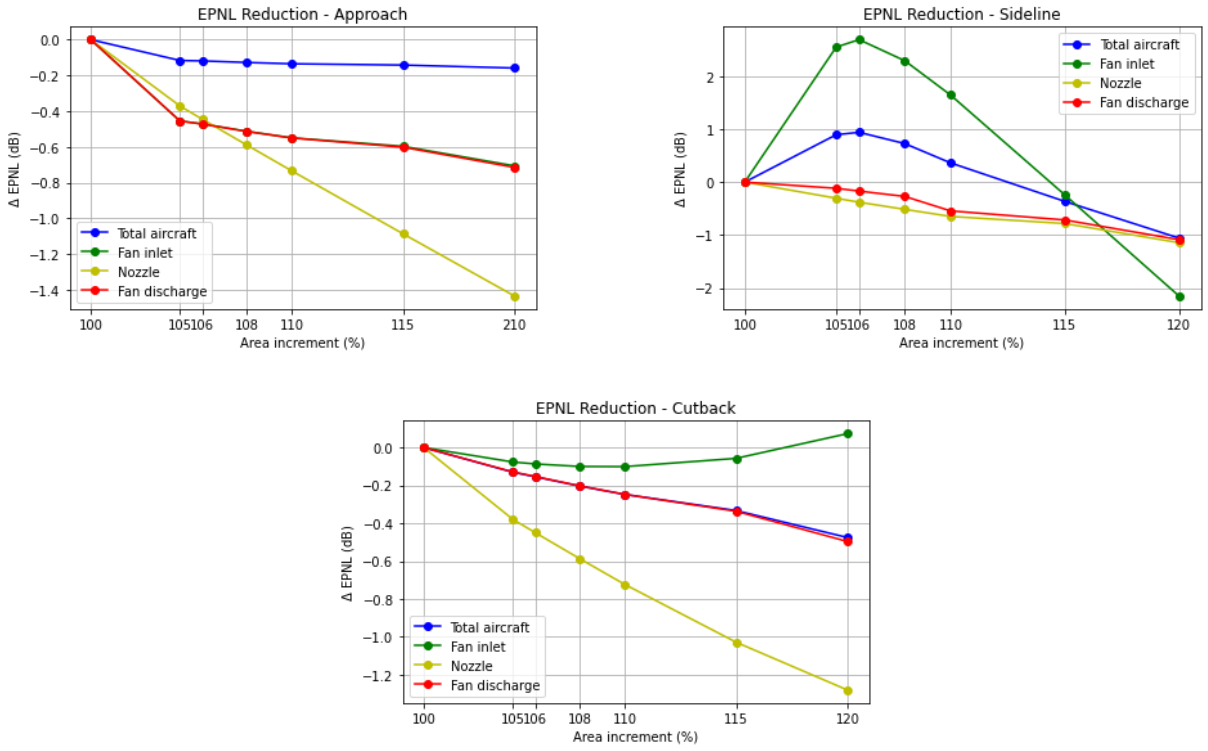

Figure 3.22: EPNL variations

Figure 3.22 represents the EPNL values for the different nozzle configurations in the three certification phases. From it, the following considerations can be made:

- The greatest reduction in nozzle EPNL is obtained with a 20 % opening in the approach phase.
- Due to the supersonic tip Mach numbers the fan inlet noise may increase and could lead to an increase in the noise of the whole aircraft as it is obtained for a 5% nozzle opening in the sideline point.
- The fan discharge EPNL follows the same trend as the jet with a lighter slope.
- The total aircraft EPNL is strictly correlated to the largest noise source, hence the total reduction for the approach phase is 0.2 dB due to the dominance of the airframe noise 3.1. The greatest aircraft noise reduction is obtained for a 20% opening in the sideline point, as this results in a reduction of 2 dB in the inlet fan noise.

3.3.3 Noise regulations

As already done for the jet and the fan the aim is now to compare the reduction in EPNL obtained with respect to other similar studies. First of all, it must be said that much has been done regarding propulsive analysis of a VAN, mechanical implementation and fan aerodynamic performance but only a few studies were dedicated to the aeroacoustic evaluation of this technology. Moreau in [49] presents the main results. In particular, [14] estimated a 2 dB reduction in jet noise with a 15% opening for sideline and cutback. On the other hand, figure 3.22 gives the following reductions for a 20% opening:

Certification point	$\Delta EPNL(dB)$
Approach	-1.4
Sideline	-1.3
Cutback	-1

Table 3.2: Jet noise EPNL reduction for 20% nozzle openings

For the fan instead, [12] observed from the NASA SDT fan noise tests a reduction of 2 dB overall sound power level, with reductions in fan noise of 3 and 5 dB with an area opening of 5% and 11% respectively. Reporting again the greatest reductions achieved in our study 3.3 and 3.5, we note that the results are less pronounced than expected.

Certification point	$\Delta EPNL(dB)$
Approach	-0.7 ($\Delta A = 20\%$)
Sideline	-2.1 ($\Delta A = 20\%$)
Cutback	-0.1 ($\Delta A = 8\%$)

Table 3.3: Fan inlet EPNL reduction for different nozzle openings

Certification point	$\Delta EPNL(dB)$
Approach	-0.7 ($\Delta A = 20\%$)
Sideline	-1 ($\Delta A = 20\%$)
Cutback	-0.43 ($\Delta A = 20\%$)

Table 3.4: Fan discharge EPNL reduction for different nozzle openings

For what concerns the total aircraft, the following results are obtained:

Certification point	$EPNL(dB)(\Delta A = 0\%)$	$EPNL(dB)(\Delta A = 20\%)$
Approach	96.9455	96.7866
Sideline	90.1327	89.0190
Cutback	89.4043	88.9287

Table 3.5: EPNL reduction for different nozzle openings

Figure 3.23 represents the EPNL limitations provided by ICAO in [20]. Chapter 4 is applicable for new type designs from 2006 and requires that the sum of the differences between maximum noise levels and permitted maximum noise levels of Chapter 3 must not be less than 10 EPNdB (cumulative margin of 10 EPNdB relative to Chapter 3), therefore an average reduction of 3.3 dB at every measurement point [50].

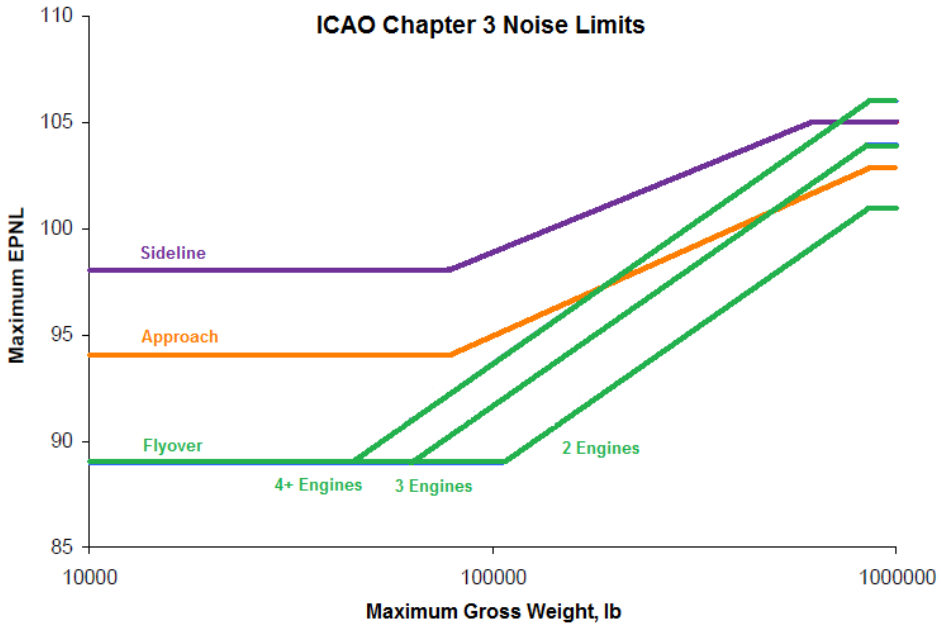

Figure 3.23: ICAO certification limits [18]

The maximum take off mass considered for the NASA CRM-HL is 297500 kg, therefore the maximum EPNL values are:

Certification point	max $EPNL(dB)$
Approach	105
Sideline	102.5
Cutback	101

Comparing these limitations with the EPNL computed in our study we see that the aircraft respects the noise limitations, and the nozzle opening increases the cumulative margin.

4 Conclusions and future developments

An aeroacoustic analysis of a UHBR engine with a VAN was carried out by analysing the source and propagated spectra for the jet and fan noise. For each nozzle opening, the engine operating point was recalculated at a fixed thrust. This made it possible to determine the variations in noise emission due to the change in bypass area. Later, the airframe noise was included to obtain the total EPNL at the different noise certification points. The results showed a reduction in jet noise with nozzle openings due to the reduction in jet velocities, reaching up to -1.4 dB in the approach phase. A 5% nozzle opening in the sideline was found to increase fan noise by more than 2 dB, resulting in an increase in total aircraft noise. Further openings instead showed a reduction of -2 dB. The reductions in the total EPNL for sideline and cutback are 1.1 dB and 0.5 dB, respectively. Qualitatively, the results are in line with theoretical expectations, which predicted a reduction of 2 dB for sideline and cutback with a 15% nozzle opening. Combining our results with the noise regulations, we find that VAN can be one of the possible technologies for noise reduction. The limitations of the study are mainly related to the fact that the exact internal geometry of the engine is not yet available and to the limitations of the code itself. In fact, CHOICE has an uncertainty of 1.5 dB from the validation tests. Furthermore, these validation tests were performed on a specific aircraft in an approach procedure. Finally, the comparisons presented in Chapter 3 refer to different geometries and for the VAN reductions they are mostly analytical. Consequently, no precise statement can be made about the level of accuracy of the study. During the study, it became evident that analysing aircraft noise is a complex task that requires consideration from various perspectives. It is also necessary to examine how this issue fits into a broader analysis, taking into account emissions, efficiency, air traffic regulations, and the mechanical implementation of the nozzle mechanism. Future developments of the study could include a more precise geometry of the engine, the use of more accurate methods and programs, and could also include propulsion efficiency considerations to provide a multidisciplinary discussion.

BIBLIOGRAPHY

[1] M. Nöding and L. Bertsch, "Application of noise certification regulations within conceptual aircraft design," *Aerospace*, vol. 8, no. 8, 2021.

[2] EASA, "Aircraft noise - easa eco, https://www.easa.europa.eu/eco/eaer/topics/technology-and-design/aircraft-noise,"

[3] L. Leifsson, "Multidisciplinary design optimization of low-noise transport aircraft [electronic resource] /," 01 2006.

[4] R. Woodward, C. Hughes, and G. Podboy, *Aeroacoustic Analysis of Fan Noise Reduction with Increased Bypass Nozzle Area*.

[5] U. Iemma and F. Centracchio, "Sound-quality-based decision making in multiobjective optimisation of operations for sustainable airport scenarios," *Aerospace*, vol. 9, no. 6, 2022.

[6] J. Vassberg, M. Dehaan, M. Rivers, and R. Wahls, "Development of a common research model for applied cfd validation studies," 08 2008.

[7] E. Maria Thoma, T. Grönstedt, E. Otero Sola, and X. Zhao, "Assessment of an open-source aircraft noise prediction model using approach phase measurements," *Journal of Aircraft*, 2023.

[8] T. Raef, A. Elzahaby, and M. Khalil, "Enhancement of propulsion performance through jet noise reduction technologies: A review," 05 2014.

[9] "LES predictions of jet noise and jet surface interactions." `https://www.craft-tech.com/applications/acoustics/`.

[10] H. Bu, X. Huang, and X. Zhang, "An overview of testing methods for aeroengine fan noise," *Progress in Aerospace Sciences*, vol. 124, p. 100722, 2021.

[11] E. M. Thoma, *Physics-based Modelling for Aircraft Noise and Emission Predictions*. PhD thesis, 2022.

[12] C. E. Hughes, G. G. Podboy, R. P. Woodward, and R. J. Jeracki, *The Effect of Bypass Nozzle Exit Area on Fan Aerodynamic Performance and Noise in a Model Turbofan Simulator*. NASA.

[13] `https://eaglepubs.erau.edu/introductiontoaerospaceflightvehicles/chapter/climbing-ceiling-gliding/`. Climbing, ceiling and gliding.

[14] U. Michel, "The benefits of variable area fan nozzles on turbofan engines," 01 2011.

[15] A. Vieira, B. von den Hoff, M. Snellen, and D. G. Simons, "Comparison of semi-empirical noise models with flyover measurements of operating aircraft," *Journal of Aircraft*, vol. 59, no. 6, p. 1574 – 1587, 2022.

[16] J. R. Stone, E. A. Krejsa, and B. J. Clark, *Jet Noise Modeling for Suppressed and Unsuppressed Aircraft in Simulated Flight*. NASA.

[17] A. Moreau, "Theoretical acoustic benefit of high bypass ratio and variable-area nozzle in turbofan engines," *14th European Conference on Turbomachinery Fluid dynamics Thermodynamics*, 2021.

[18] Jayaraman and Shankar, "Dynamic cutback optimization,"

[19] A. L. Sylvain Mouton, Grégoire Charpentier, "Test summary of the full-span high-lift common research model at the onera f1 pressurized low-speed wind tunnel," *AIAA SciTech Forum*, 2023.

[20] International Civil Aviation Organization (ICAO), *Annex 16 – Environmental protection*. ICAO, 2017.

[21] M. Basner, W. Babisch, A. Davis, M. Brink, C. Clark, S. Janssen, and S. Stansfeld, "Auditory and non-auditory effects of noise on health," *The Lancet*, vol. 383, no. 9925, pp. 1325–1332, 2014.

[22] A. Filippone, "Aircraft noise prediction," *Progress in Aerospace Sciences*, vol. 68, pp. 27–63, 2014.

[23] A. Hirschberg and S. Rienstra, "An introduction to aeroacoustics," vol. 1823, pp. 18–7, 08 2004.

[24] J. Delfs, "Lecture notes in basics of aeroacoustics," October 2021.

[25] C. A. Hall, E. Schwartz, and J. I. Hileman, "Assessment of technologies for the silent aircraft initiative," *Journal of Propulsion and Power*, vol. 25, no. 6, pp. 1153–1162, 2009.

[26] International Civil Aviation Organization (ICAO), "Icao noise reduction technology," https://www.icao.int/environmental-protection/Pages/Noise-Reduction-Technology.aspx.

[27] G. Krishnan, C. Perullo, and D. Mavris, "An assessment of relative technology benefits of a variable pitch fan and variable area nozzle," 07 2013.

[28] J. Hileman, T. Reynolds, T. Law, and S. Thomas, "Development of approach procedures for silent aircraft," vol. 8, 01 2007.

[29] O. Cots, J. Gergaud, and D. Goubinat, "Direct and indirect methods in optimal control with state constraints and the climbing trajectory of an aircraft," *Optimal Control Applications and Methods*, vol. 39, 11 2017.

[30] International Civil Aviation Organization, *Environmental Technical Manual*. ICAO, 2015. Procedures for the Noise Certification of Aircraft.

[31] L. Lopes and C. Burley, "Design of the next generation aircraft noise prediction program: Anopp2," 06 2011.

[32] L. Bertsch, "Parametric aircraft noise analysis module - status overview and recent applications,"

[33] I. H. Joachim Kurzke, *Propulsion and Power*. Springer Cham.

[34] "Choice github link: https://github.com/emthm/choice.git," `https://github.com/emthm/CHOICE`.

[35] U. Tengzelius and A. Johansson, ""aircraft noise mapping code saft"," vol. Centre for Sustainable Aviation, 2021.

[36] R. Ji, X. Huang, and X. Zhao, "Active jet noise control of turbofan engine based on explicit model predictive control," *Applied Sciences*, vol. 12, no. 10, 2022.

[37] J. Russell, "An empirical method for predicting the mixing noise levelsof subsonic circular and coaxial jets," *NASA Langley Research Center, NASA-CR3786*, 1984.

[38] M. F. Heidmann, "Interim prediction method for fan and compressor source noise," tech. rep., NASA-TM-X-71763 Lewis Research Center, Cleveland, Ohio, 1979.

[39] K. B. Kontos, B. A. Janardan, and P. R. Gliebe., "Improved nasa-anopp noise prediction computer code for advanced subsonic propulsion systems.," tech. rep., Cincinnati, OH United States: NASA Lewis Research Center, 1996.

[40] P. Gliebe, R. Mani, H. Shin, B. Mitchell, G. Ashford, S. Salamah, and S. Connell, "Aeroacoustic prediction codes.," tech. rep., Contractor Report NASA/CR-2000- 210244. Glenn Research Center: NASA, 2000.

[41] D. G. Dunn and N. A. Peart, "Aircraft noise source and contour estimation," tech. rep., Contractor Report (CR) NASA-CR-114649. Boeing Commercial Airplane Co. Seattle, WA, United States: NASA, 1973.

[42] https://commonresearchmodel.larc.nasa.gov/high-lift-crm/. NASA Common Research Model (CRM).

[43] Y. Guo, "Empirical prediction of aircraft landing gear noise," tech. rep., Boeing Phantom Works, Long Beach, California. NASA/CR-2005-213780, 2005.

[44] International Civil Aviation Organization, "Procedures for air navigation services - Aircraft Operations," vol. Voulme I, 2018.

[45] A. Magrini, G. Subbian, R. Radespiel, and E. Benini, "Powered turbofan effects on aircraft aerodynamics at high-lift: A study on the nasa crm-hl," *Aerospace Science and Technology*, vol. 144, p. 108825, 2024.

[46] J. Sun, J. Hoekstra, and J. Ellerbroek, "Aircraft drag polar estimation based on a stochastic hierarchical model," 2018.

[47] International Civil Aviation Organization, "Continuous climb operations (cco) manual," vol. DOC 993.

[48] E. A. Krejsa and J. R. Stone, *Enhanced Fan Noise Modeling for Turbofan Engines*. NASA.

[49] A. Moreau, R. Schnell, and M. Mennicken, "Acoustic preliminary design of a low-noise fan stage considering a variable-area nozzle and variable-pitch rotor blades," *CEAS Aeronautical Journal*, vol. 14, 04 2023.

[50] P. Hullah, B. Figlar, G. Öttl, S. Schwanke, R. Rodríguez, T. Gjestland, A. Gühnemann, H. Harwatt, M. Tight, and G. Benderli, "State of the art on tradable permits, noise legislation, noise restriction methods and noise modelling," 02 2014.

ACKNOWLEDGEMENT

" The supervisor of this thesis was supported by the PHD@UNIPD programme of the Foundation Cariparo under the project ANTENORE-Advanced iNvestigaTion at off-dEsigN Operation of uhbpR Engines."